

POLITECNICO DI TORINO

Collegio di Ingegneria Chimica e dei Materiali

**Corso di Laurea Magistrale
in Ingegneria dei Materiali**

Tesi di Laurea Magistrale

Degradazione di inquinanti acquiferi contenenti azoto



Relatore

prof. Barbara Bonelli (DISAT)
Freyria Francesca Stefania (Docente esterno)

.....
.....

Candidato

Blangetti Nicola

Novembre 2018

Summary

I. Riassunto	Errore. Il segnalibro non è definito.
Abstract	1
Introduction	2
1. Photo catalysis	4
1.1 Materials for Photo catalysis	6
1.2 TiO ₂	8
1.3 Synthesis of materials	10
1.3.1 Sol gel method	11
1.3.2 Hydrothermal methods	11
1.3.3 Solvothermal Technique	11
2. Pollutants and Pesticides	13
2.1 General introduction about pollution due to pesticides	14
2.1.1 Pesticides and herbicides	15
2.2 Atrazine and simazine	16
2.3 Simazine byproducts	17
2.4 Fenton's like reaction	19
3. Powder characterization techniques	21
3.1 X-ray powder diffraction technique (XRPD)	21
3.1.1 The instrument	21
3.1.2 Theory	21
3.1.3 Data acquisition	22
3.1.4 Results	22
3.2 Adsorption-Desorption isotherms of N ₂ at 77 K (BET)	23
3.3 Catalytic properties	26
3.3.1 Theory	26
3.3.2 Procedures	27
3.3.3 Results	27
3.4 Transmission electron microscopy (TEM)	28
3.4.1 Theory	28
3.4.2 Procedure	29
3.5 Infrared spectroscopy (IR)	30
3.5.1 Transmission infrared spectroscopy	32

4. Synthesis and materials	33
4.1 Synthesis n°1: mesoporous titanium dioxide	33
4.1.1 Direct method with Fe (MesTiO ₂ dirFe)	34
4.2 Synthesis n°2: brookite synthesis	34
4.3 Materials and characterization results	35
4.3.1 Mesoporous titanium dioxide calcined at 450°C (MesTiO ₂ _450)	35
4.3.2 Mesoporous titanium dioxide calcined at 700°C (MesTiO ₂ _700)	37
4.3.3 Mesoporous titanium dioxide calcined at 900°C (MesTiO ₂ _900)	38
4.3.4 Mesoporous Titanium dioxide direct synthesis with Fe (MesTiO ₂ dirFe)	40
4.3.5 Second method of synthesis for titanium dioxide (B1_200)	42
4.3.6 Second method of synthesis for titanium dioxide (B1_600)	44
4.5. Quantitative material analysis results.....	47
4.5.1 Rietveld analysis results	47
4.5.2 Band gap investigation	48
4.5.3 Crystallites dimension investigation.....	48
4.6 Conclusions	49
5. Photocatalytic tests.....	51
5.1 Experimental settings	51
5.1.1 Catalyst.....	51
5.1.2 H ₂ O ₂ usage for photocatalytic analysis.	51
5.1.3 Simazine concentration	52
5.1.4 Lamps and reactor	52
5.2 Blank experiments:.....	54
5.2.1 tests without catalyst.....	54
5.2.2 Simazine photolysis.....	54
5.2.3 H ₂ O ₂ interaction with simazine	55
5.3 Photo catalysis tests in presence of photo-catalytic materials.....	56
5.3.1 Solution n°1 MestiO ₂ _450 H ₂ O ₂	56
5.3.2 Solution n°1 MestiO ₂ dirFe H ₂ O ₂	57
5.3.3 Solution n°1 Degussa P25 H ₂ O ₂	58
5.3.4 Solution n°2 MestiO ₂ _450 H ₂ O ₂	59
5.3.5 Solution n°2 MesTiO ₂ _900	60
5.3.6 Solution n°2 B1_200	61
5.3.7 Solution n°2 B1_200 Subtracted	62
5.3.8 Solution n°2 B1_200_600	63

5.3.9 Solution n°2 B1_600	64
5.3.10 Solution n°2 B1_200 0,5g/L.....	65
5.4 Solution n°2 MesTiO ₂ _450 UV	66
Conclusions	67
Bibliography.....	70

I. Riassunto

I.1 introduzione

La gestione delle acque reflue è attualmente un problema e lo sarà sempre di più dal momento che la popolazione mondiale e la produzione industriale e agricola mostra un andamento crescente.

In molti casi le acque utilizzate in ambito domestico provengono da acque reflue che devono dunque essere trattate in maniera adeguata. Tra tutti gli inquinanti la cui presenza viene riscontrata nelle acque una classe particolare è quella dei contaminanti emergenti.

I contaminanti emergenti sono quegli inquinanti presenti in tracce che non vengono eliminati dai convenzionali metodi di depurazione delle acque.

I contaminanti emergenti sono considerati pericolosi per le loro caratteristiche tossicologiche, chimiche e, nonostante un quantitativo minimo sia tollerato dagli esseri umani, non è sempre chiara la quantità accettabile per le acque potabili. Fig 1.6 illustra schematicamente gli inquinanti ascrivibili come inquinanti emergenti.[1]

Main Categories	Families	Examples
Drugs and Pharmaceuticals	antibiotics/antibacterials	amoxicillin, metronidazole, ofloxacin
	steroids	estrone, 17 β -estradiol, testosterone
	β -blocker	propranolol, salbutamol, atenolol
	nonsteroidal anti-inflammatory drugs (NSAID)	aspirin, ibuprofen, naproxen, ketoprofen
	antiepileptic/anticonvulsants	gabapentin, carbamazepine
	antidepressant/hypnotic	diazepam, venlafaxine, amitriptyline, dosulepin, meprobanate
	analgesic	morphine, propoxyphene, paracetamol
	hypertension	valsartan
	lipid regulation	bezafibrate, simvastatin, clofibrac acid
	erectile dysfunction	sildenafil
Stimulant and generally illegal drugs	hallucinogen	3,4-Methylenedioxyamphetamine (MDMA), 3,4-Methylenedioxy-N-ethylamphetamine (MDEA), 3,4-Methylenedioxyamphetamine (MDA)
	stimulant	amphetamine, cocaine, benzylpiperazine
	human indicator	caffeine, nicotine
Personal care products	preservative	methylparaben, propylparaben
	sunscreen agent	1-benzophenone, homosalate
	disinfectants/antiseptic	chloramines, chlorine, chlorine dioxide, chlorhexidine digluconate
	fragrances	musk xylol, tonalide
Pesticides/Herbicides	organohalogenated compounds	Dichlorodiphenyltrichloroethane (DDT), lindane, vinclozolin, clopyralid
	nitrogen containing	simazine, phenylurea

Figure 1.6 inquinanti emergent

Gli inquinanti emergenti qui riportati sono difficili da eliminare con i convenzionali metodi di trattamento delle acque. Per questo motivo la concentrazione di inquinanti di questo tipo sta raggiungendo livelli allarmanti.

Tra tutti i contaminanti gli erbicidi costituiscono una importante classe di sostanze il cui utilizzo è in continua crescita da anni.

Il lavoro svolto ha riguardato lo studio della degradazione mediante fotocatalisi di un erbicida denominato simazina. Questo erbicida appartiene alla famiglia delle triazine e dunque è costituito da una struttura ciclica di 6 atomi di azoto e carbonio con sostituenti posizionati in posizione 1,3 e 5 dell'anello.

Gli studi di fotocatalisi presentati nel lavoro sono stati effettuati con l'utilizzo di fotocatalizzatori sempre costituiti da biossido di titanio (TiO_2)

Gli studi di fotocatalisi presentati nel lavoro sono stati effettuati con l'utilizzo di catalizzatori sempre costituiti da biossido di titanio opportunamente sintetizzato. Le polveri sono state sintetizzate seguendo due metodi sol gel diversi. In un caso è stato utilizzato un template al fine di indurre la formazione di una struttura mesoporosa. Nell'altro caso non è stato utilizzato il template ma è stata modulata composizione delle fasi cristalline mediante il controllo del pH. Un materiale dopato con Fe ma prodotto seguendo il metodo sol-gel tradizionale è anche stato caratterizzato e provato in test fotocatalitici.

Le polveri sono poi state caratterizzate mediante:

- Analisi XRPD per definire le fasi cristallografiche presenti.
- Isotherme di adsorbimento e desorbimento di azoto a -77K per indagare le proprietà superficiali e la porosità dei materiali
- DR UV-Vis per determinare l'energy gap dei materiali
- Spettroscopia FTIR per indagare la presenza di fasi organiche sulle polveri.
- Microscopia TEM per determinare dimensione e forma delle fasi cristalline.

I principali risultati delle prove elencate precedentemente possono essere riassunti dicendo che i materiali sintetizzati presentano strutture mesoporose con cristalli di dimensioni nanometriche nel caso della sintesi con componente template. Nel caso della sintesi senza template sono stati prodotti materiali che presentano le tre principali strutture allotropiche della titania rutilo, anatasio e brookite. I risultati della caratterizzazione sono stati confrontati con un TiO_2 commerciale, Degussa P25 il quale è una miscela di rutilo e anatasio. Le due fasi cristallografiche sono presenti in proporzione del 19% nel caso del rutilo e dell'81% nel caso dell'anatasio. La P25 presenta inoltre bassa porosità con un'area specifica superficiale di $50 \text{ m}^2/\text{g}$.

I campioni sintetizzati e caratterizzati sono poi stati utilizzati per effettuare le prove di fotocatalisi al fine di degradare la simazina.

Le prove sono state effettuate variando alcuni parametri sperimentali. In questo modo è stato possibile identificare sia le condizioni ideali per la degradazione della simazina che le caratteristiche richieste al catalizzatore per poter incentivare la reazione con l'inquinante.

Tutte le prove di fotocatalisi sono state svolte seguendo la medesima procedura. Il procedimento seguito è consistito nella preparazione della soluzione e poi nell'irraggiamento del reattore per 240 minuti. Durante la prova vengono effettuati campionamenti ogni 60 minuti e in seguito la soluzione è analizzata mediante lo spettrofotometro UV-Vis per seguire l'andamento della

reazione monitorando lo spostamento o la variazione di intensità dei picchi caratteristici della simazina.

I.II TiO_2 come fotocatalizzatore

La fotocatalisi è un ramo della catalisi in cui la velocità di reazione (o la sua inializzazione) è garantita o incentivata dalla azione della luce ultravioletta, visibile o infrarossa.

La radiazione luminosa quando viene assorbita dal materiale induce la generazione di coppie elettroni lacune (e^-/h^+). I portatori di carica così generati possono subire vari percorsi:

- Possono interagire con le molecole inquinanti a contatto con la superficie generando una reazione o sia ossidativa o riduttiva[2]
- Essere soggetti a ricombinazione, cioè all'annichilimento delle cariche.
- Possono rimanere intrappolati in livelli intermedi presenti nell' energy gap la cui profondità impedisce ai portatori di interagire con gli inquinanti sulla superficie.

Queste possibilità sono comuni a tutti i semiconduttori e sono motivo di indagine nel mondo della fotocatalisi.

La scelta dei fotocatalizzatori va eseguita in base alle caratteristiche chimico-fisiche degli stessi con particolare attenzione alle caratteristiche di interazione con la luce e alle caratteristiche superficiali del materiale che deve interagire con l'inquinante.

Per modificare l'assorbimento della luce da parte del materiale si può ricorrere alla introduzione di atomi dopanti all'interno del reticolo che possono variare l'ampiezza dell'energy gap o introdurre livelli intermedi.

E' da considerare anche la possibilità di modificare le proprietà elettroniche dei materiali mediante modifica delle caratteristiche cristallografiche, delle dimensione dei cristalli e della presenza di interfacce di fase tra diverse strutture cristalline. [3]

I.II.I TiO_2

Il biossido di titanio è il semiconduttore più utilizzato per applicazioni fotocatalitiche.[4] Il successo di questo materiale è legato alle sue proprietà:

- Atossicità
- Assenza di solubilità in acqua
- Basso costo
- Alta inerzia chimica

Le più comuni forme allotropiche della titania sono anatasio, rutilo e brookite. La differenza tra le tre forme cristalline è la diversa disposizione nello spazio degli ottaedri TiO_6 . Questa induce distorsioni negli stessi implica la generazione di diversi livelli elettronici per ogni forma allotropica della titania.

La stabilità delle varie fasi è legata anche alla dimensione dei cristalli, il rutilo termodinamicamente stabile quando i cristalli sono di dimensione maggiore ai 35 nm. I cristalli di brookite sono da considerarsi stabili quando la loro dimensione è compresa tra gli 11nm e i 35 nm. Infine l'anatasio è termodinamicamente stabile per cristalli al di sotto degli 11 nm.

Le proprietà fotocatalitiche della titania sono influenzate dalle fasi cristalline presenti. In particolare Ohtani et al. [5] ha dimostrato come, con cristalli di dimensione nanometrica, la brookite presenti proprietà fotocatalitiche migliori dell'anatasio o della miscela anatasio-rutilo. Altri studi hanno dimostrato le proprietà fotocatalitiche della brookite come Vequizo et all [3] che correla la efficienza fotocatalitica con la possibilità di avere livelli intermedi nel band gap.

I.II Inquinanti contenenti azoto

Gli inquinanti contenenti azoto di origine umana sono un problema sempre più importante perché sono di difficile eliminazione con i tradizionali metodi di depurazione delle acque.[1]

I principali inquinanti contenenti azoto sono pesticidi/erbicidi, coloranti e farmaci per uso umano e veterinario.

Il lavoro di tesi è stato incentrato sulla degradazione della simazina che è un erbicida della famiglia delle triazine. Le triazine sono costituite da un anello composto da sei atomi tre di carbonio e tre di azoto con il posizionamento dei sostituenti che può variare in base al sottogruppo. La simazina presenta sostituenti in posizione 1,3 e 5. Fig 2.4 mostra una rappresentazione della molecola di simazina

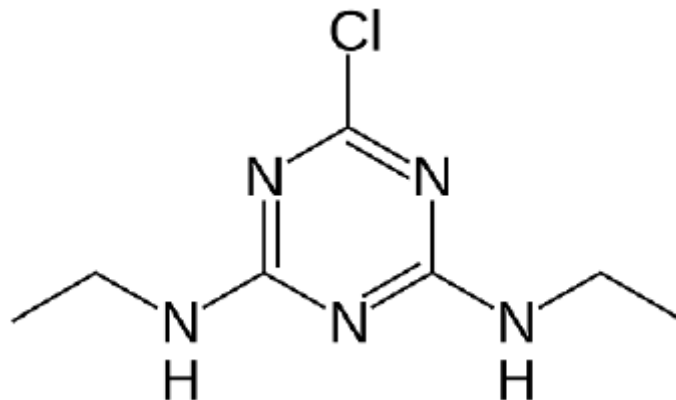


Figura 2.4 molecola di simazine

La simazina è considerata una sostanza pericolosa per il sistema endocrino oltre che cancerogena.

I rischi correlati con questa sostanza hanno spinto l'EPA e la Commissione Europea a istituire dei limiti massimi di concentrazione di simazina nelle acque potabili. Il limite in Europa è di 0.1 µg/L mentre negli USA è di 4 µg/L.

La degradazione alla molecola di simazina può avvenire secondo vari step e percorsi ma si possono evidenziare due fenomeni:

- Perdita del sostituito cloro e conseguente idrossilazione.
- De alchilazione dei sostituenti in posizione 3 e 5

Per monitorare l'andamento della degradazione durante i test di fotocatalisi è stata utilizzata la spettroscopia UV-Vis. In fig 3.6 è proposto lo spettro di assorbimento della simazina dispersa in acqua

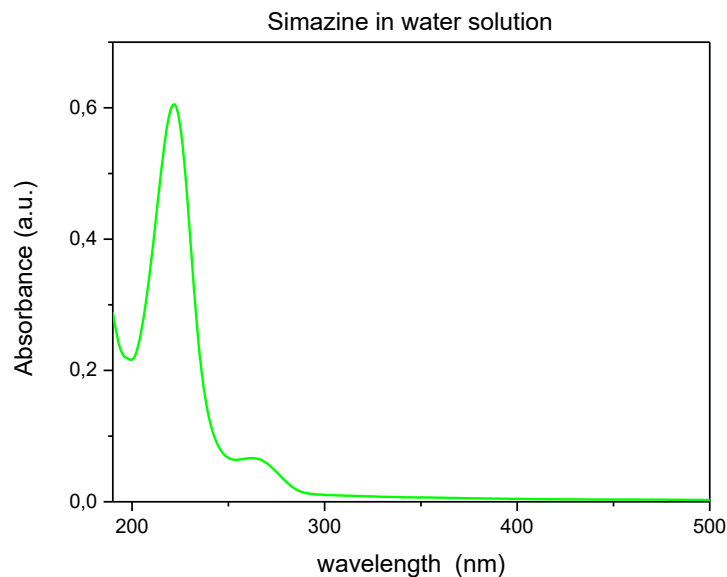


Figure 3.6 Simazine in soluzione acquosa

- Banda principale a 221 nm legata a transizioni elettroniche interne all'anello ($\pi \rightarrow \pi^*$).
- Banda secondaria, di minore intensità, a 270 nm legata alle catene laterali. ($n \rightarrow \pi^*$).

I.II.I Sottoprodotti della simazina

In base alla letteratura una via per degradare la simazina è ricorrere a quelli che vengono definiti meccanismi di ossidazione avanzati (AOP) che riguardano varie tecniche tra cui la fotocatalisi.

L'effetto della fotocatalisi può essere incrementato con l'ausilio del perossido di idrogeno (H_2O_2) il quale interagendo con la luce genera radicali, in particolare ossidrilici i quali attaccano la molecola di simazina. Nel momento in cui questa azione dell' H_2O_2 è combinata con la presenza di atomi di Fe (come avviene con il nostro campione dopato con Fe) può avere luogo la reazione di Fenton. Questo meccanismo costituisce un promettente metodo per la degradazione degli inquinanti dato il basso costo e basso impatto ambientale.

I.III sintesi e caratterizzazione dei materiali

La sintesi dei fotocatalizzatori è stata effettuata seguendo due diversi metodi e le temperature di calcinazione sono state scelte in modo da modificare le caratteristiche del materiale dal punto di vista della struttura cristallina.

I.III.I la sintesi

La prima sintesi ha portato alla produzione di un materiale mesoporoso mediante un metodo sol-gel. I principali reagenti utilizzati sono un copolimero a blocchi (Pluronic P123) e Butossido di Titanio come precursore.

La calcinazione è stata effettuata a 450°C, 700°C e 900°C con rampa termica di 1,8 °C/min e con un mantenimento di 4h a quella temperatura. I campioni prodotti con questo metodo sono riassunti nel seguente elenco

- 700 °C (MesTiO₂700)
- 900°C(MesTiO₂900)
- 450°C(MesTiO₂_450)

Il catalizzatore dopato con Fe è stato ottenuto mediante lo stesso metodo di sintesi ma in questo caso sono stati introdotti 2.5g del cloruro ferrico FeCl₃·H₂O durante la sintesi. La temperatura di calcinazione scelta è stata di 450°C. E' stato così ottenuto un materiale con 2.5%wt di Fe

L'altro metodo di sintesi sviluppato da Mutuma et al [6] porta alla formazione di un materiale con composizione cristallografica particolare dal momento che nel materiale finale sono presenti le tre principali strutture allotropiche della titania.

Il metodo non prevede l'uso del templante. Il precursore è il titanio isopropossido con utilizzo di alcool isopropilico e acido nitrico per modulare il pH durante la sintesi. La calcinazione è stata effettuata con rampa termica di 5°C/min con mantenimento in temperatura per 5 ore. Le temperature di calcinazione scelte sono 200°C e 600°C. I campioni prodotti sono proposti nel seguente elenco:

- 200 °C (B1_200)
- 600 °C (B1_600)
- 200°C e poi 600°C (B1_200_600)

I.III.II Caratterizzazione dei materiali

I materiali sono stati caratterizzati mediante:

- Analisi XRPD con conseguente elaborazione dei diffrattogrammi mediante il metodo di raffinamento di Rietveld.
- Spettroscopia TEM
- Spettroscopia DR-UV-Vis
- Isoterma di assorbimento e desorbimento di N₂

I risultati espressi in forma completa sono riportati nel capitolo 4

Dalla analisi dei diffrattogrammi è stato possibile determinare le fasi cristalline presenti nei campioni e mediante il raffinamento Rietveld si è potuto anche determinare la percentuale in cui queste fasi sono presenti. Tab 4.9 riporta i risultati della elaborazione mediante Rietveld dei campioni sintetizzati

Table 4.9 percentuali fasi cristalline

Sample	B1_200	B1_200_600	B1_600	MesTiO ₂ _700	MesTiO ₂ _900	P25	MesTiO ₂ _450
anatase	77%	84,60%	82,10 %	100%	95,9%	81%	100%
brookite e	23%	10,50%	10,40 %		4,10%		
rutile		4,90%	7,40%			19%	

Le isoterme di assorbimento e desorbimento di azoto hanno fornito come informazione l'area superficiale specifica secondo il modello BET e la distribuzione dei pori mediante il modello BJH applicato alla isoterma di desorbimento.

Table I isoterma di adsorbimento e desorbimento

<i>Sample</i>	<i>BET specific surface area (m²/g)</i>	<i>BJH desorption mean pore value(nm)</i>
<i>MesTiO₂_450</i>	139	9
<i>MesTiO₂_700</i>	14	[7.5]
<i>MesTiO₂_900</i>	1	6.3
<i>MesTiO₂dirFe</i>	129	6.1
<i>BI_200</i>	207	5
<i>BI_600</i>	31	9
<i>BI_200_600</i>	37	10

La spettroscopia DR-UV-Vis fornisce uno spettro che è stato elaborato ed è stato espresso come Tauc Plot. Dal Tauc plot è possibile ricavare l'entità del band gap. Vengono riportati i valori misurati relativi al band gap diretto e indiretto. Vanno considerati entrambi dal momento che il materiale è costituito da più fasi cristalline. Il rutilo presenta gap indiretto così come la brookite ma l'anatasio ha gap diretto.

Table 4.10 band gap

<i>Sample</i>	<i>Direct gap(eV)</i>	<i>Indirect gap(eV)</i>
<i>BI_200</i>	3,11	3,44
<i>BI_200_600</i>	2,97	3,11
<i>BI_600</i>	3	2,52
<i>MesTiO₂_700</i>	3,0	
<i>MesTiO₂_900</i>	3,25	3,15
<i>P25</i>	3	3,64

La microscopia TEM è stata utilizzata per determinare la dimensione dei cristalli mediante il diametro di Feret e la deviazione standard. Tab 4.11 riporta i valori misurati con ImageJ

Table 4.10 diametro di feret medio e deviazione standard

<i>Sample</i>	<i>Mean d_F value(nm)</i>	<i>Standard Deviation</i>
<i>BI_200</i>	7	0,8
<i>BI_200_600</i>	25	3
<i>MesTiO₂_900</i>	111	21

I.II.IV Conclusioni caratterizzazione

La sintesi numero 1 porta alla formazione di anatasio con alta area superficiale specifica, struttura mesoporosa e una omogenea morfologia delle particelle. Ad una temperatura di calcinazione maggiore (900°C) si è notata la presenza di rutilo mentre si è riscontrato un grande decremento della area superficiale.

La sintesi numero 2 la quale non prevede l'uso del tempelante porta ad avere un mix di strutture allotropiche della titania. L'area superficiale specifica nel caso della calcinazione a 200 °C è la più elevata tra tutti i materiali presentati. Con l'aumentare della temperatura di calcinazione si ha transizione da brookite ad anatasio e rutilo. Inoltre si ha un decremento dell'area superficiale.

I.IV Test di fotocatalisi

Le prove di fotocatalisi sono state eseguite seguendo la stessa procedura:

- Preparazione soluzione contenente simazina
- Dispersione del fotocatalizzatore all'interno della soluzione.
- Attesa di un ora in cui il reattore contenente la soluzione con catalizzatore è mantenuto isolato dalla luce (dark)
- Irraggiamento con lampada per 240 min e campionamento ogni 60 min di un campione di soluzione da analizzare con lo spettrofotometro UV-Vis

Il campione di soluzione prima di essere analizzato con lo spettrofotometro è stato centrifugato a 4000 rpm per 12 minuti.

.

Gli aspetti variati durante le prove sono:

- Tipo catalizzatore
- Concentrazione del catalizzatore
- Concentrazione della simazina
- Concentrazione H₂O₂
- Sorgente luminosa (lampada con radiazione UV o solare)

I risultati più interessanti delle prove di fotocatalisi sono proposti in seguito e verranno confrontati con gli spettri ottenuti dalla prova con P25 in presenza di perossido di idrogeno (fig 5.6). Questo risultato è considerato come modello per due ragioni: per prima cosa per via della riconosciuta efficacia del catalizzatore P25. In secondo luogo la presenza di perossido di idrogeno rende la prova teoricamente più efficace dal punto di vista fotocatalitico e' altresì vero che solo una piccola parte del perossido di idrogeno viene ridotto in radicali in seguito alla illuminazione. L'effetto più importante del H₂O₂ che abbiamo riscontrato è stato con presenza di Fe nel catalizzatore.

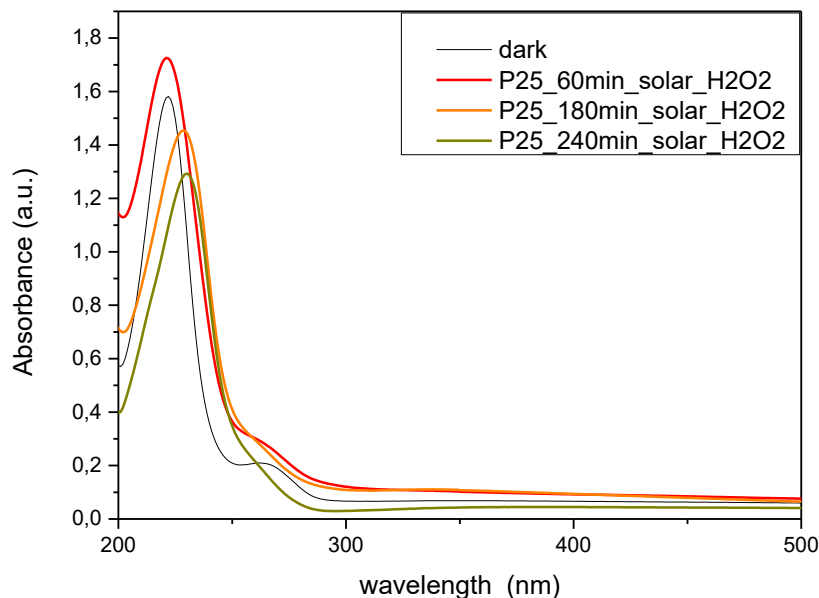


Figure 5.6 degradazione simazina in presenza di P25 e perossido di idrogeno

La degradazione della simazina in presenza di P25 procede seguendo due meccanismi visibili in Fig5.6. Il picco principale a 221 nm mostra uno spostamento verso lunghezze d'onda maggiori e questo spostamento è dovuto alla perdita del sostituente Cl e successiva idrossilazione dell'anello.

Allo stesso tempo è possibile notare come il picco attorno a 270 nm mostri una variazione di forma con il passare del tempo di irraggiamento. Questo fenomeno è legato alla perdita dei sostituenti laterali.

In seguito sono proposti gli spettri di assorbimento della prova effettuata con B1_200 come catalizzatore e senza la presenza di perossido di idrogeno irraggiati con lampada solare Fig (5.10)

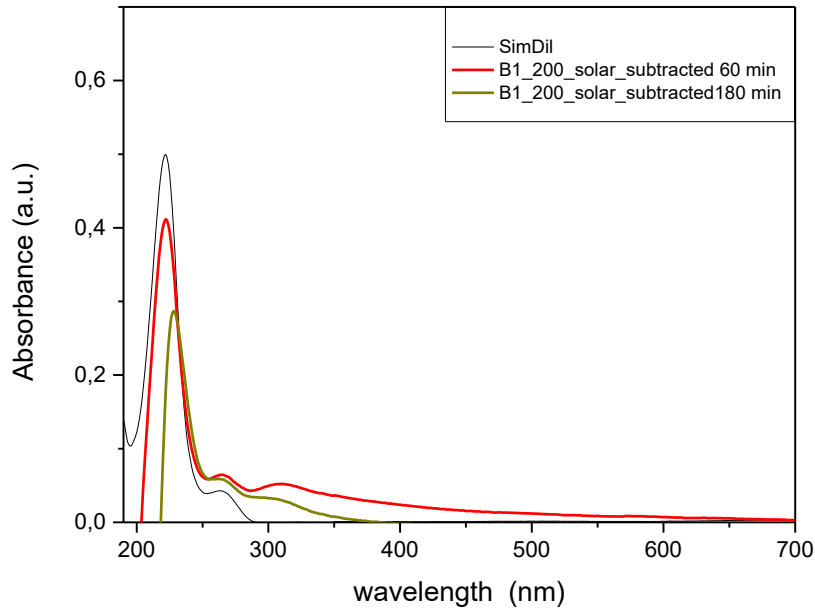


Figure 5.10 B1_200 in soluzione di simazina lampada solare

Fig 5.10 mostra come anche con l'azione del catalizzatore B1_200 costituito da brookite, rutilo e anatasio sia possibile ottenere uno spostamento significativo del picco a 221nm. Come abbiamo visto lo stesso comportamento è stato riscontrato durante la prova con P25. In questo caso, inoltre; non si utilizza l' H_2O_2 . Per questi motivi si può considerare molto efficace il nostro materiale.

Infine sono presentati gli spettri di assorbimento(fig5.8) della prova di fotocatalisi effettuata con MesTiO₂_900 come catalizzatore. La radiazione scelta è stata quella della lampada che simula la radiazione .solare Non è stato utilizzato perossido di idrogeno.

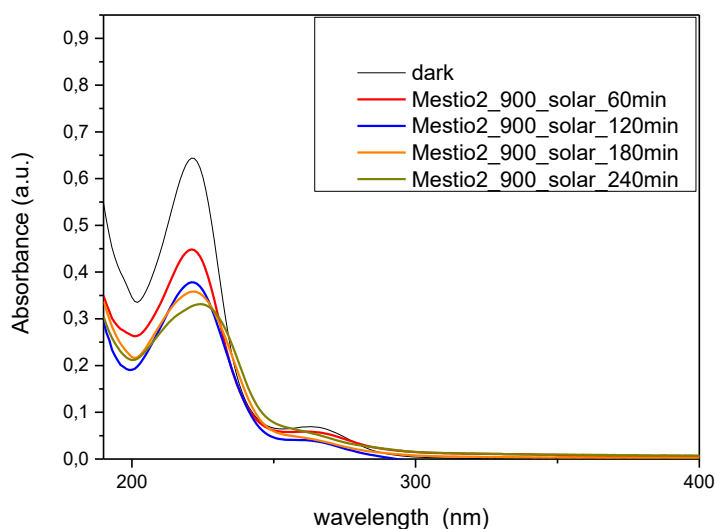


Figure 5.8 mesTiO₂_900 in soluzione di simazina radiazione solare

In Fig 5.8 è possibile osservare una significativa diminuzione di assorbanza del picco caratteristico della simazina a 221nm. Si evidenzia, inoltre, una variazione della forma della banda caratteristica dovuta alla sovrapposizione di più bande di assorbimento. Queste bande sono legate a sottoprodotti della degradazione della simazina.

I.V conclusioni

Il nostro lavoro si è focalizzato sullo studio nei numerosi aspetti che influenzano la degradazione per via fotocatalitica di un inquinante presente nelle acque chiamato simazina.

I catalizzatori sintetizzati sono stati studiati e ottimizzati per ottenere un mix di caratteristiche microstrutturali e morfologiche al fine di incentivare la reazione di fotocatalisi.

Le sintesi proposte con le conseguenti temperature di calcinazione garantiscono la scelta tra varie configurazioni.

Diversi aspetti sono stati modificati durante la prova di fotocatalisi e il confronto tra i risultati dimostra che siamo in grado di incentivare un meccanismo di degradazione piuttosto che un altro scegliendo un materiale.

I risultati più interessanti sono stati ottenuti utilizzando il catalizzatore definito dal nome B1_200 che presenta efficacia paragonabile alla P25 pur presentando caratteristiche morfologiche e cristallografiche diverse.

La B1_200 presenta alta area superficiale specifica ed inoltre al suo interno sono presenti molte interfacce di fase che secondo la letteratura limitano la ricombinazione dei portatori. Queste due caratteristiche sono in linea con l'efficacia del catalizzatore.

La prova con MesTiO₂_900 dimostra che questo materiale nonostante la bassa area superficiale specifica è efficace nella degradazione. Anche in questo caso sono presenti interfacce di fase.

La degradazione completa della simazina non è stata ottenuta ma una degradazione anche parziale è evidente osservando i risultati dei test fotocatalitici.

Per maggiore consapevolezza dei fenomeni che avvengono durante i test fotocatalitici sarebbe importante eseguire test di cromatografia come l'HPLC

Abstract

In aquatic environment, it is possible to find a noteworthy number of emerging pollutants (Eps), which are molecules that are difficult to remove by common wastewater treatment. Among these N-containing pollutants are particularly dangerous.

The aim of the thesis is the preparation and study of TiO₂ based photo-catalysts (pure and doped with Fe) for the photocatalytic degradation of N-containing pollutant, such as simazine. The simazine is a common herbicide, (6-chloro-N,N-diethyl-1,3,5-triazine-2,4-diamine), which belongs to the triazine family, characterized by six-atoms rings containing three carbon and nitrogen atoms.

Several catalytic materials are synthesised and characterized in order to compare material properties, tuned by synthesis pathways, and photocatalytic efficiency. . In order to investigate morphological and microstructural properties XRPD spectroscopy N₂ adsorption-desorption isotherm results are proposed. TEM images and FTIR reports are proposed as well. Band gap analysis with diffuse reflectance-UV-Vis spectroscopy is proposed. Synthesised materials characterization showed mesoporous structures with crystallites dimension between 7nm and 100 nm. Specific surface area of samples produced with modified sol gel synthesis method showed SSA of 207m²/g. XRPD analysis showed mixed allotropic phase materials where anatase rutile and brookite were detected. Possible configuration are enlisted below:

- Anatase
- Anatase-rutile
- Anatase brookite-rutile
- Anatase doped with Fe

A commercial TiO₂ (Degussa P25) was used as term of comparison.

The effect of previously described configurations and properties have been studied in photocatalytic tests where H₂O₂ concentration, simazine concentration and type of illumination (solar light vs UV) were variated.

. Investigation about photocatalytic degradation of simazine in different condition offers information about catalyst properties

Different reaction mechanisms have been found, depending on both chemical composition(doping presence) and synthesis method.

Introduction

Water treatment will be one of the most important field of study in the next years because of population growth and growing industrialization worldwide. There are many methods to process wastewater in order to reduce pollutants or dangerous microorganisms. According to WHO an improper management of water pollution can lead to health problems like infections, diseases etc.

Therefore urban, industrial and agricultural wastewater inadequate treatment is an important issue as long as drinking water of hundreds of million people come from re-use of these water sources. Nowadays treated water is dangerously contaminated or it contains trace of chemical pollutants.

Among pollutants, an important class is defined as emerging contaminants (ECs) because data concerning their fate, transport, toxicity and tolerated concentration in water for human usage are not completely available. ECs are basically either naturally occurring or synthesized substances that interfere with organisms endocrine systems and result in unnatural responses of them [1].

Pesticides and herbicides can be classified as emerging pollutants. Simazine is an herbicide product that has a maximum allowed amount in nature ($1\mu\text{g/L}$) and is classified as eco toxic for plants and algae and carcinogenic for humans.

We propose photocatalytic methods to reduce simazine amount by utilizing TiO_2 based semiconductors as catalyst and solar light as activating source.

We synthesized different kind of mesoporous TiO_2 following different synthesis methods with the aim of investigate how crystallographic and morphological changes can influence the photo degradation of simazine.

Photo catalysis tests are proposed where experimental settings were modified in order to evaluate catalysts efficiency in simazine degradation processes.

The present thesis is divided in 6 chapters:

Chapter 1; Brief description of photo catalysis materials and properties. Focus on TiO_2 properties and allotropic phases is proposed.

Chapter 2; Introduction on different families of pollutants and degradation technologies. Explanation about simazine, chemical description and possible degradation pathways. Focus on photolysis, photo catalysis and the Fenton reaction is proposed.

Chapter 3; Characterization techniques are briefly described. Analysis settings is proposed as well. Crystallographic composition is analysed with XRPD analysis. Morphology is investigated with. N_2 adsorption and desorption isotherms (77K). UV-Vis spectroscopy is described for photocatalytic test monitoring. FTIR analysis and TEM microscopy are proposed as well

Chapter 4; Material synthesis methods are proposed. Characterization of materials results with graphs and tables are listed and they are compared. Brief conclusion of synthesis and characterization chapter is proposed as well.

Chapter 5; Photocatalytic tests of simazine degradation are proposed. Photo catalysis tests settings like hydrogen peroxide presence and simazine concentration are varied and UV-Vis spectroscopy spectra are utilized to follow degradation processes.

Chapter 6; conclusions and future perspective

1. Photo catalysis

A catalyst is a substance that make a chemical reaction faster without modifying overall Gibbs energy ($\Delta G = \Delta H - T\Delta S$) change of the reaction. The processes that involve catalysts are called catalysis[2]

There are two kind of catalysis:

- Homogeneous catalysis in which just one phase is involved.
- Heterogeneous catalysis in which chemical reaction take place at the interface between phases. Photo catalysis is a branch of catalysis where the chemical reaction rate (or its initiation) is guaranteed or aided by the action of ultraviolet, visible or infrared solar radiation. Fig1.1 proposed below is a schematic description of photocatalytic mechanism[3]

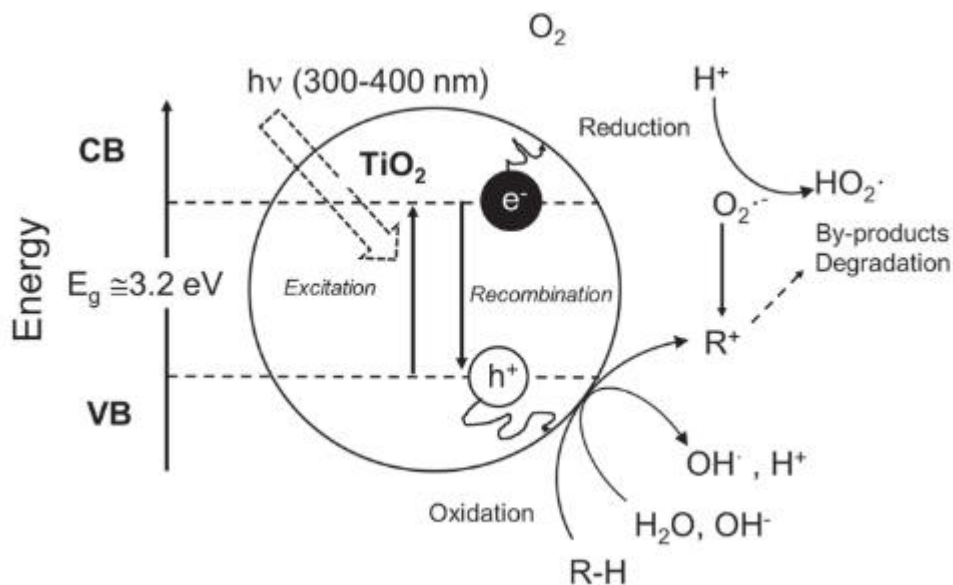


Figure 1.1 schematic representation of photo catalysis mechanism

.Catalyst utilized in photocatalytic process is named photo catalyst and it can enhance degradation of pollutants kinetics when activated by charge separation between conductive and valence band. Electronic displacement is consequence of photon absorption.[2]

Photo catalysis is a chemical/physical process has been acquiring research interest since the publication of Fujima et all paper in 1972 [4] in which a TiO₂ electrode (with a Platinum counter-electrode) has been used for solar energy conversion and storage.

Many studies have been following that papers and nowadays Generation of charge species and surface phenomena have been understood but the process is still not completely resolved .[5][6]

The basic mechanism is photon adsorption that induces promotion to conduction band of one electron, which leaves a hole in valence band.

Photo generated carriers can undergo many pathways:

- Recombination when electron and hole annihilate each other and restore pre-photon electronic situation.
- Trapping in intermediate levels within energy gap, it can be a deep trap or shallow one and it will influence if carriers may interact or not.
- Carriers can reach the surface and induce predict reactions.

Last pathway describes the best photo catalyst mechanism where photo-generated carriers can reach the surface and they can react with molecules adsorbed on the surface, which in our case are pollutant molecules

Electrons and holes are suitable to cause reduction and oxidation respectively as Figure1 schematically shows.[7]

Depends on some physical-chemical properties of a photo catalyst surface, such as the surface charge, some pollutants are weakly adsorbed on the surface and so molecular properties are important as well..

When oxidation due to charge carriers is not enough powerful, indirect oxidation is needed: this mechanism is based on production of $\text{OH}\cdot$ radicals that start oxidation of molecules in liquid phase.

It is possible to introduce hydrogen peroxide inside photo catalysis reactor to get the same goal of indirect oxidation. Usually, $\text{OH}\cdot$ radicals attack aromatic rings.

Many issues are linked to material when it is studied in a microscopic scale and they are listed below:

- Crystallographic phase
- Crystallites size
- Dopant presence

These parameters are described as intrinsic ones.

On the Other hand is possible to underline many other aspects categorized as extrinsic and the most important are enlisted below[6]:

- pH of the solution.
- Concentration of pollutants.
- Light intensity
- Catalyst dosage

1.1 Materials for Photo catalysis

Semiconducting materials are of great interest in environmental remediation processes due to their possibility to generate charge carriers when activated by a proper energy. During photocatalytic processes, activating energy derives from light beam that arrives on semiconductors. Light absorption properties and excited lifetimes as long as electronic structure are consequently important characteristics of semiconducting materials for photocatalytic applications.[7]. Therefore, semiconductor material for heterogeneous photo catalysis should have:

- An appropriate band gap
- High carriers mobility
- Non toxicity
- Chemical stability

One of the most important property is electronic structure that is deeply linked to orbitals of single atoms composing materials and interatomic bonding. Electronic structure of atoms included in a crystal take place in band structure that is the combination of atomic orbitals and properties due to organise lattice.

Materials composed by atoms of same type do not have electrons surplus or deficit. When two type of atoms are present and some defects within lattice structure take place it is possible to have some electric equilibrium alteration. Presence of electrons not involved in interatomic bonding leads to n-type materials, which have deficit of holes. Opposite situation guarantee a p-type material in which electrons are less than equilibrium while holes are majority carriers.

In our study we focused on TiO₂ based materials but for photo catalysis, it is possible to use many types of semiconductors. That is possible thanks to electronic band structure of these materials and in particular their ability to promote electron to conduction band (CB) which leave free holes in valence band (VB) separation when excited by light. As it is written before, there are many kinds of semiconductors depending on different properties. We studied TiO₂ that is classified as n-type semiconductors that means majority of carriers are electrons thanks to a small deficit of O atoms compensated by Ti adopting 3+ oxidation state[7].

Another n-type semiconductors is ZnO that is the second most employed semiconductors although undergoes degradation in acid pH solution conditions and so it does not respect chemical stability criteria.[8]. Despite that problem, ZnO is a promising material for photo catalysis. Photocatalytic properties of ZnO depends on preparation method because different band structure are due to presence of defects like twins.[9]

Another semiconductor is Cu₂O, it is a p-type semiconductors that according to Ramirez et al[7]has been studied for water splitting and so energy conversion applications.[10] The problem of this material is chemical stability in aqueous solution because the redox potentials for the reduction and oxidation of monovalent copper oxide lie within the bandgap[11]

WO₃ is quite effective when irradiated with laser beam. Although that it is a photo catalyst high recombination rate of carriers generated by light exposure of material photo-induced. High recombination rate is a quite common problem and with our research work we tried to propose some pathways with purpose of reducing it for TiO₂. [12]

More complex and more recent photo catalysts are based on ternary or quaternary structures.

Among these new compounds is important to cite

- Vanadates [7]
- Bi_2WO_6 and BiMoO_6 that have showed effective properties to inactivate E.coli[13]

These materials can be possible alternatives to TiO_2 , to overcome some of titanium dioxide drawbacks like electron-hole recombination and small number of visible photons that can be absorbed, many efforts have been done . An example of this pathway is TiO_2 lattice doping [8].

It is possible to add different kinds of atoms to TiO_2 depending on which property is needed to improve. There are three different schemes that a semiconductors can pursue when doped as shown in Figure 1.2 [14]:

- Lower shift of valence band due to introduction of electron donor doping agent. Fermi level is closer to valence band instead of conduction band.
- Upper shift of conduction band due to hole donor doping atoms introduction. Fermi level is close to conduction band.
- Impurity introduce level within band gap.

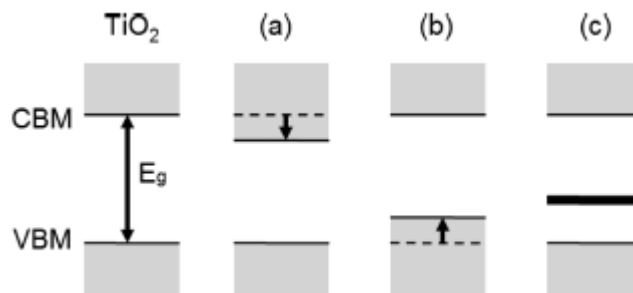


Figure 1.2 a) A lower shift of Conduction Band, b) An upper shift of Valence Band, c) Impurity shift in the band Gap

Last possibility proposed In Figure 1.2 could cause problems when electronic levels shifts are too deep and so electrons cannot take part of reaction on the surface. Levels displacement due to impurity can work as recombination site for electrons and holes and so their lifetime can be too short. Other aspects of this problem are described in chapter 1.3

Dopants atoms can be divided in metals and non-metals heteroatoms.

Among non-metals atoms, *e.g.* sulphur, carbon, Iodine, phosphorous and nitrogen Latter is the element that confers better properties and increases visible light absorption. TiO_2 behaviours when doped with Nitrogen atoms are similar to what happen when sulphur atoms are utilized but in N case is easier to incorporate them into O site . Nitrogen atoms can be interstitial or substitutional or can even form oxides that substitutes O atoms[14]. Doping with metals can be another option compared to non-metals dopingbecause bottom edge of conduction band consists of Ti d states and so substitutional doping of transition metal with d orbitals suitable to be introduced within conduction band can induce a upper shift of valence band[14]. Talking

about crystallography we can assume that Fe^{3+} (0,64 Å) and Ti^{4+} (0,68 Å) can interchange without inducing significant alteration of crystal structure.[15] Other advantage of Fe doping are listed below

- Nontoxic.
- Easy to add during Synthesis and to include within lattice structure.
- Quite cheap compared for example to Gold(Au)
- It can promote Fenton's reaction
- It improves Visible Photon absorption that means it causes a reduction of Band Gap.

During our work we doped mesoporous titanium dioxide with iron (Fe) with the purpose of benefit from all these advantages and description of that are proposed in chapter 2.4.1

Doping is important because it modifies photonic efficiency as well. [7]

1.2 TiO_2

Titanium oxide has been the most used materials for photocatalytic application, according to (García-lópez et all) [8] between 2008 and 2011 around 75% of publications about this field are related to TiO_2 and possible modification of its properties. Main characteristics that explain why so much studies has been done about this material are:

- Nontoxicity,
- Water insolubility
- Hydrophilicity ,
- Low cost (for common TiO_2),
- Chemical stability and resistance to photo corrosion.

TiO_2 is a binary oxide and has three main different allotropic structures as shown in Fig 1.3[16]

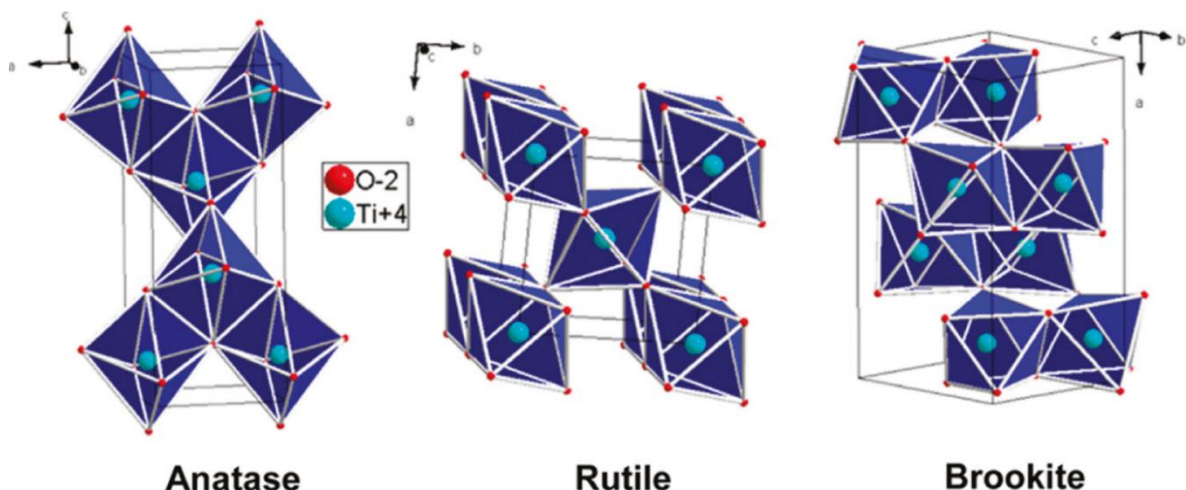


Figure 1.3 TiO_6 octahedron disposition

. In Fig 1.3 it is possible to observe that octahedron TiO_6 units show peculiar distortions and they share different corners and edges. It is possible to resume the wholes structures as follow [7]

- Anatase (tetragonal, D_{4h}^{19} -I41/amd, $a=b=3.782 \text{ \AA}$, $c=9.502 \text{ \AA}$)
- Rutile (tetragonal, D_4^{14} -P42/mnm, $a=b=4.584 \text{ \AA}$, $c=2.953 \text{ \AA}$)
- Brookite (rhombohedral, D_{2h}^{15} -Pbca, $a=5.436 \text{ \AA}$, $b=9.166 \text{ \AA}$, $c=5.135 \text{ \AA}$)

Among three allotropic structures, anatase and rutile are the most studied and commonly are recognised as the two most important species in photo catalysis. As consequence of that there are also many studies on electronic band structures of these materials according to which the different distortions of octahedrons lead to different electronic levels allowed and so a peculiar band gap structure Fig1.4[17]

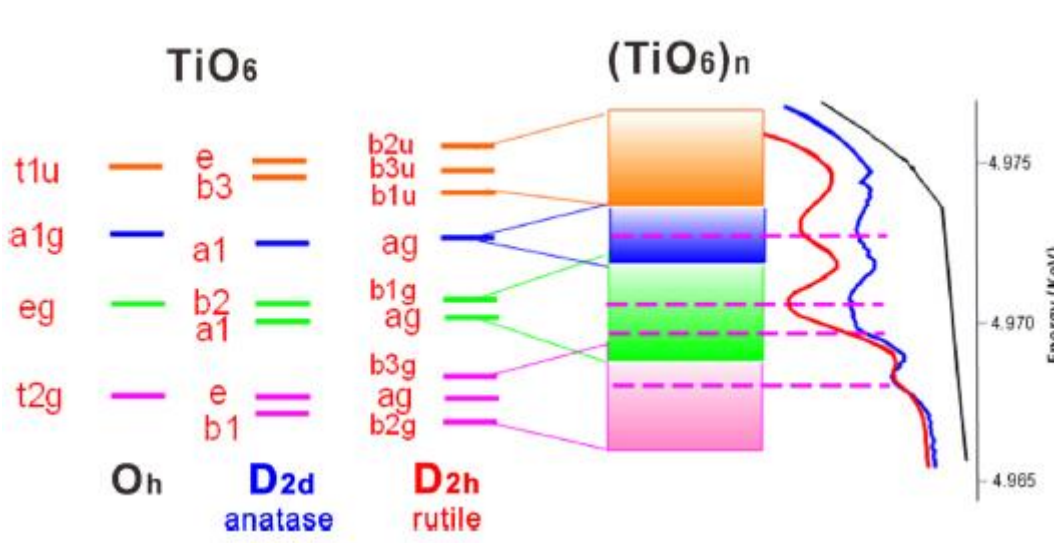


Figure 1.4 anatase and rutile band structure

Different crystalline structures show also differences in the band gap type and structure. Anatase has an indirect band gap that means that transition of electrons from Valence Band (VB) to Conduction Band (CB) needs a change of crystalline momentum as long as energy to promote electrons to valence band but on the other hand it means that recombination of photo-excited carriers will take place later. On the other hand brookite and rutile have direct band gap .[18]

Brookite is another allotropic structure that has been less studied. Reason for this overlook is phase stability of crystallites that for anatase phase is below 11 nm while brookite has stable crystallites between 11 and 35 nm. . When the material is heated the final state is rutile and it suggests that it's thermodynamically most stable phase[19]. Fig1.4 shows electronic levels of rutile and anatase phases.

As long as we focused on mesoporous TiO₂ anatase was commonly obtained. Mesoporous TiO₂ is a promising material for photocatalytic applications thanks to the high specific surface area that allows pollutant/products to reach the surface and in particular is enhanced the possibility to reach reactive sites in order to improve photocatalytic efficiency.

Our work brings under attention phase transformation and photocatalytic effectiveness of different allotropic structures. We analysed brookite that according to (Ohtani et al) [20] when dimension of crystallites is nanometric would have better photocatalytic activities than pure anatase or anatase and rutile configurations.

In order to confirm the previous theory, it is important to take into consideration (Vequizo et al) [21] in which a photocatalytic activity is correlated with presence of intermediate allowed electronic levels within band gap. What they underline is that these levels act as electronic trap when the separation of electrons and holes happen after photon absorption in order to make recombination charge carriers less probable. When electron confinement happens, free holes would be able to induce oxidation of molecules adsorbed to the surface while, at the same time, electron moderately trapped can react as well with pollutant molecules.

Intermediate levels are due to defect and so are typical of every atomic structure [21]:

- Anatase has electron-traps very shallow with at less than Kt (<0,1 eV) energy separation and so contribution is no valuable.
- Rutile has deepest (0,9eV) intermediate levels of three phases and so electrons are almost no reactive.
- Brookite shows electron-traps with intermediate deepness (around 0,4eV) that would allow reaction of both carriers and so even reduction and oxidation could take place.

Brookite appears as the best photo catalyst according to what is written in the paper but another aspect should be taken into consideration that is free-life time of electrons and their ability to reduce pollutants molecules brookite traps shorten too much the period in which electrons can react and so life of electrons is very short (around ps) [21]. anatase defects allows longer time compared to brookite and so reduction ability is higher but on the other hand recombination rate is the highest of three allotropic structures. Therefore, brookite and anatase show similar efficiency but for different mechanisms.

As mentioned above electrons reaction ability is important because when holes take part into oxidation, and so are consumed, trapped electrons would start to recombine if pollutant reduction cannot take place. What described before happens with rutile structure. [21]

1.3 Synthesis of materials

Production of Titanium oxide for photocatalytic application has been deeply studied since property of this material has been discovered. We will focus on bottom-up approach because we pay attention to produce nanometric-organised materials instead of top down - methods that start from TiO₂ blocks and arrive to powders. Synthesis strategy as long as precursors and reactants choice is important because these parameters can alter size of particles and their allotropic structure. As explained in chapter 1.3 allotropic structure will influence adsorption of pollutants and electron transfer rate. [22]

There are mainly four ways to obtain a TiO₂ with nanometrically-organised particles. Other method liked direct oxidation of titanium as long as PVD and CVD methods are feasible but we prefer to focus on technique that we used during laboratory work or that are similar to them.

A brief resume of production techniques is proposed in order to understand what we did.

1.3.1 Sol gel method

Sol-gel methods are based on the transformation of a sol into a gel which is dried and most of the time calcined to obtain final material. A sol is a solution of the precursor compounds that contain Titanium atoms. Precursor solution undergoes treatments of chemical and thermal type that lead to metal-oxygen bonds which cause network formation within liquid phase. Bonded structure is called Gel. Hydrolysis and growth speed of precursor can be modified with acidic or base added to solutions and consequently crystallinity and particles size can be controlled in some way. Is possible to add polymers that act as a substrate upon which nuclei can grow.[22]

1.3.2 Hydrothermal methods

The word hydrothermal commonly refers to any heterogeneous reaction in which an aqueous solvents or a mineralizers under high temperature and pressure condition is present.[23] Focusing on photo catalysis in autoclave to obtain TiO₂, it is commonly added titanium precursor previously peptized. After that, a process under pressure at a relative high temperature is followed.

1.3.3 Solvothermal Technique

Solvothermal method derives from hydrothermal method but solvent is not aqueous. The main consequence is that mechanism has to be different from hydrolysis and condensation. No hydrolytic method where water absence leads to oxidation with oxygen belonging to other compounds. On the other hand, in non-aqueous methods water is generated during reactions. Advantage of this technique is better control of size, shape, distribution and crystallinity of particles compared to hydrothermal method because hydrolysis commonly is too quick.

Fig 1.5 resumes some synthesis methods for porous titanium dioxide and their properties[24]

Synthesis routes	Template	P_s TiO ₂ /nm	TiO ₂ phase	S_{BET}/m^2g^{-1}	$V_p/cm^3 g^{-1}$	Dp/nm	Pollutants	Ref.	
Sol-gel	CTAB	5	A	340	0.28	3.2	Rh6G	29	
			A	281		5	MB, BP, MO	30	
			A	262		4	2-Propanol	45	
	Tween	9.2	A	147	0.221	4	MB, <i>E. coli</i>	57	
			A	91.7			0.187	7-9	Stearic acid
	P104	5-7	A + R	175	0.187	4.5	Phenol	27	
			A	171			CH ₃ Br	58	
	P123	13.2	A + R	200	0.187	4.6	Benzene	33	
			A + R	34			6.7	HCHO and MB	37
	Hydrothermal	Polymer brush	12 ± 2	A	34	0.4	2.2	RhB	36
				A	174			10-110	MO
		SiO ₂ microspheres	2.2 μm	A	214	0.61	2.5	<i>E. coli</i>	60
A + B				140	RhB and phenol			47	
PEO and PEG		10	A	168	0.35	7.6	RhB	48	
			A + B	156			RhB	50	
CTAB		6-11	A	71	0.35	20	Acetone	44	
			B + R	140			RhB	46	
None		300	A	140	0.35	8	MB	55	
			A + B	140			CH ₃ CHO	56	
TEA		10	A + R	90.4	0.15	5	MB	52	
			A	112			0.24	6.7	<i>n</i> -Pentane
TMAH	10	A	112	0.24	6.7	<i>n</i> -Pentane	53 and 54		
		A + B	112			0.24	6.7	<i>n</i> -Pentane	53 and 54
None	15	A + R	140	0.15	5	MB	52		
		A	90.4			0.15	5	MB	52
TDA	100	A	90.4	0.15	5	MB	52		
		A	90.4			0.15	5	MB	52
P123	7.7	A + B	112	0.24	6.7	<i>n</i> -Pentane	53 and 54		
		A + B	112			0.24	6.7	<i>n</i> -Pentane	53 and 54

^a Methyl orange (MO), bromopyrogallol red (BP), methylene blue (MB), *Escherichia coli* (*E. coli*), Rhodamine B (RhB), Rhodamine 6G (Rh6G), tetramethylammoniumhydroxide (TMAH), poly-(ethylene oxide)-poly(propylene oxide)-poly(ethyleneoxide) (EO_x-PO_yEO_x), EO₁₈PO₅₈EO₁₈

Figure 1.5 synthesis methods

2. Pollutants and Pesticides

Humans have been fighting against various pests since they started to farm (2500 BC). In the last two centuries, through chemistry many new pesticides have been developed. Recently, for various reasons among which the population growth, in order to produce adequate supplies of food, chemical pesticides and herbicides have been intensively applied.

Pesticides are "chemicals used to kill a species or a group of species that causes trouble, annoyance or destruction" [3]

Pesticides can be divided in three major classes of products: insecticides, fungicides, and herbicides, specifically, are used for control of weeds.[23]

Herbicides classification take into account chemical composition and mode of action. We focused on nitrogen containing pollutants called triazine described in chapter 2.3

Fig 2.1 shows pesticides production [UN food and agricultural organization FAO]

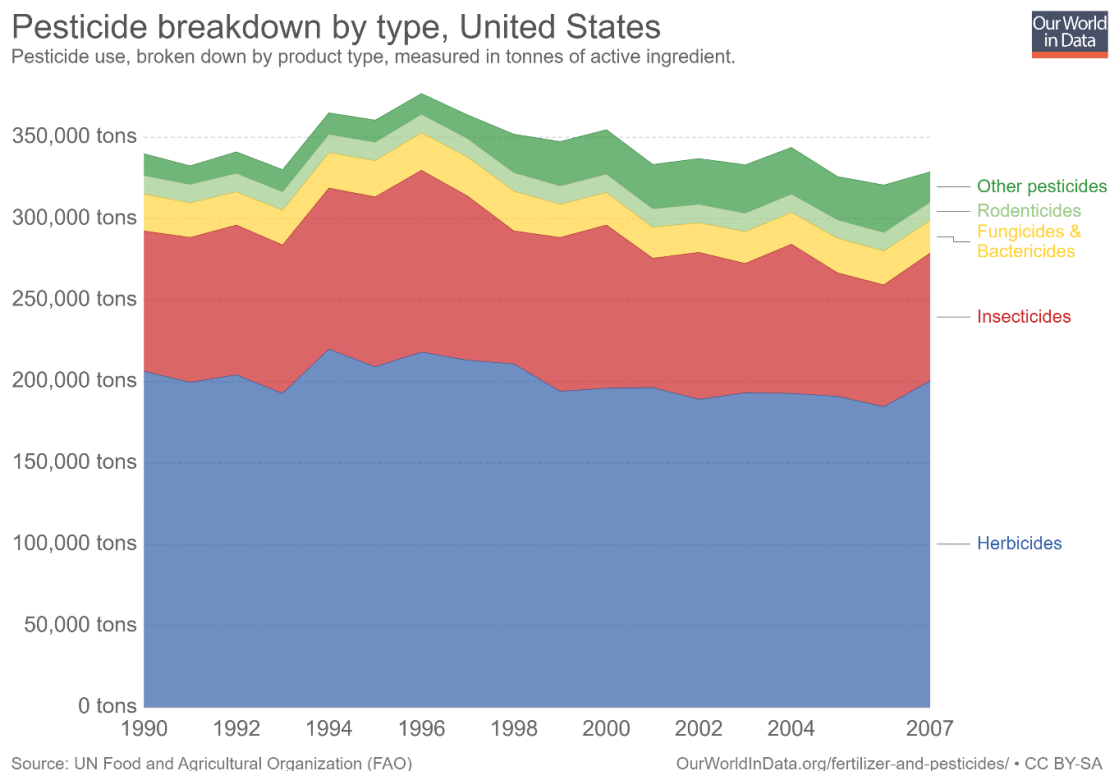


Figure 2.1 Pesticides subdivision

2.1 General introduction about pollution due to pesticides

Contamination of water is an important issue nowadays. Pollution is increasing because of population growth and this can have many consequences like:

- Increasing demand of food and so spread of pesticides utilization in agriculture activities.
- Increase of Pharmaceuticals use.
- Industrial activities increase and consequently more waste water production.

Among pollutants of anthropogenic origin, N-containing ones are quite diffuse and are namely dyes, pesticides/herbicides and pharmaceuticals. These chemicals and their metabolites in case of drugs are responsible of water pollution because of their high solubility and low adsorption in soil. Drugs are described as emerging pollutants because most of decontamination plants cannot treat them but abundance of traces in water, which is increasing nowadays, is making them toxic. [1][3].

Fig 2.2 shows a classification of emerging pollutants proposed by Freyria et al[1]

Main Categories	Families	Examples
Drugs and Pharmaceuticals	antibiotics/antibacterials	amoxicillin, metronidazole, ofloxacin
	steroids	estrone, 17 β -estradiol, testosterone
	β -blocker	propranolol, salbutamol, atenolol
	nonsteroidal anti-inflammatory drugs (NSAID)	aspirin, ibuprofen, naproxen, ketoprofen
	antiepileptic/anticonvulsants	gabapentin, carbamazepine
	antidepressant/hypnotic	diazepam, venlafaxine, amitriptyline, dosulepin, meprobanate
	analgesic	morphine, propoxyphene, paracetamol
	hypertension	valsartan
	lipid regulation	bezafibrate, simvastatin, clofibrac acid
	erectile dysfunction	sildenafil
Stimulant and generally illegal drugs	hallucinogen	3,4-Methylenedioxyamphetamine (MDMA), 3,4-Methylenedioxy-N-ethylamphetamine (MDEA), 3,4-Methylenedioxyamphetamine (MDA)
	stimulant	amphetamine, cocaine, benzylpiperazine
	human indicator	caffeine, nicotine
Personal care products	preservative	methylparaben, propylparaben
	sunscreen agent	1-benzophenone, homosalate
	disinfectants/antiseptic	chloramines, chlorine, chlorine dioxide, chlorhexidine digluconate
	fragrances	musk xylol, tonalide
		organohalogenated compounds
Pesticides/Herbicides	nitrogen containing	simazine, phenylurea

Figure 2.2 emerging pollutants

Common physical-chemical removal methods for pollutants based on adsorption, coagulation and chlorination suffer of high costs as long as production of big amount of solid or secondary

waste difficult to process and consequently released in the environment.[25] Others technique includes ozone treatment, activated carbon, carbon adsorption, microbial action, hydrolysis at low ph.

A possible alternative could be: advanced oxidation processes (AOP) based on OH· radicals interaction with pollutant molecules. These radicals begin oxidation process which can lead to complete abatement and so mineralization of molecules.[26] Mineralization is the aim of chemical oxidation processes and it means conversion of pollutants into carbon dioxide, water and inorganics.

Among processes involving light usage for water treatment, photocatalytic treatments with semiconductors able to oxidise and even to reduce pollutant molecules, have been investigated and they are receiving increasing attention because of mild conditions required and high efficiency.[27]

A common semiconductor for this purpose is TiO₂ that plays an important role in organic contamination treatment since Honda-Fujima effect has been discovered.[28]

Titanium dioxide-assisted aerobic photocatalytic reaction can be summarized as follows:

Organic contaminant \rightarrow (TiO₂, O₂, hv>E_g) \rightarrow CO₂+H₂O+ Corresponding Acid

Another important aspect is the opportunity of couple advanced oxidation process (AOP) with biological treatment when by-products of oxidation are biodegradable. Biological treatment themselves are not enough efficient but would be effective if simpler molecule would be processed[29]

As long as AOP processes take advantage of different reacting system, all of them have the common purpose of producing OH radicals and radical utilization to face many situations and requests. In our work, we applied:

- H₂O₂/Fe²⁺ (Fenton)
- H₂O₂/Fe³⁺ (Fenton-like)
- H₂O₂/Fe²⁺(Fe₃*)/UV (Photo assisted Fenton)
- TiO₂/hv/O₂ (photo catalysis)

Therefore, the (chapter 2.2) includes some explanation about how we exploited these mechanisms. Some intent of avoiding UV usage (i.e. TiO₂ doping) are proposed.

Triazine and simazine undergo photolytic destruction but high-energy photons are needed and rarely total degradation of pollutant is reached. [27]

2.1.1 Pesticides and herbicides

Since half of previous century herbicide and insecticide applications to crops have been showing a steadily increase.

One of the major problems with herbicide is the ability to drain into groundwater that are sources of drinking water.

Herbicides and pesticides are described as persistent organic pollutants (POP) due to their resistance to natural degradation processes. [30]

Approximately 50% of USA population drink water from underground sources and around 95% in USA of people from countryside collect groundwater. [31]

Due so big amount of water consumed by population that is potentially polluted many efforts have to be done in order to reduce pollutant trace inside water.

Since 1990s, Environmental Protection Agency (EPA) started to discover pollutant traces in USA underground water and this discovery as long as potential health problems for humans caused by herbicides leads to use-restrictions.

Some countries banned definitely some Pesticides and Herbicides while USA and Europe decided Maximum Contaminant Levels for many substances.[31] Among herbicides under investigation by EPA and European Commission triazine family plays an important role and because of that, we focused our study on these azo-compounds herbicides.

2.2 Atrazine and simazine

Triazine herbicides are chemical compounds that present triazine chemical group that has planar benzene-like aromatic ring with three carbons replaced by nitrogen atoms. The three isomers of triazine are distinguished by the positions of their nitrogen atoms and are referred to as 1,2,3-triazine, 1,2,4-triazine, and 1,3,5-triazine.[32]

Fig 2.3 shows the general formula of 1, 3, 5-compounds described below the image.

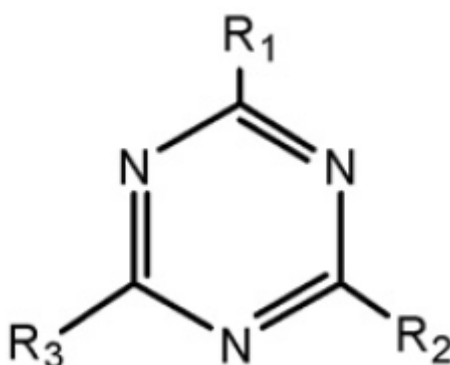


Figure 2.3 Triazine Formula[33]

Upon nitrogen based herbicides, atrazine is one of the most widely used in agriculture and forestry fields[33]. Due to its quite high solubility and its low absorption in soil, atrazine is considered a persistent organic pollutant (POP).

Persistent pollutants are an increasing problem in water pollution because such substances are not effectively removed by conventional methods.

Atrazine has been categorized as possible carcinogenic in the 1980s and nowadays medical research showed that this substance is a putative endocrine disruptor.

Consequently, European countries banned the herbicide and set a limit in drinkable water of 1µg/L and in United States USEPA organization decided for 3µg/L for USA as a maximum level in water.

Beside atrazine, another herbicide of triazine family is simazine. Fig 2.4 shows simazine molecule

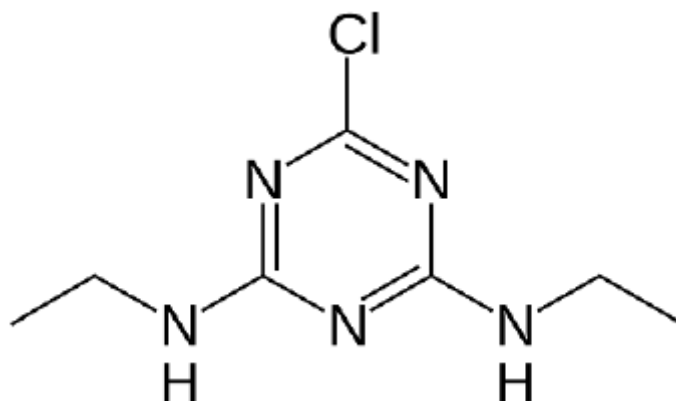


Figure 2.4 Simazine Formula

Simazine(6-chloro-N,N-diethyl-1,3,5-triazine-2,4-diamine), is a white organic solid used for control of grassy weed on deep rooted crops and farm ponds as long as fish hatcheries and fruit plants like apple and nuts[33][34] Simazine is widely used and trace of this pollutant are observed frequently with a regularity just minor of atrazine if herbicides are detected.

Aforementioned pollutant is moderately persistent in fields ground and can remain active for years in basic soils and is poorly bound to soil and so it can be washed by runoff with consequent dangerously contamination of underground water. Volatilization is insignificant as long as biodegradability.[31]

According to EPA and European Commission, simazine can cause health problems like Atrazine.

Because of high usage of Simazine and previously described properties, some countries (i.e. Norway) totally banned it. Other countries decided to establish a maximum amount of pollutant admitted of 1µg/L for Europe and 3 µg/L for USA.

2.3 Simazine byproducts

The herbicide simazine has been under investigation during our research job. Few articles in literature suggest possible degradation mechanisms and reaction pathways will be proposed in this chapter.

The whole family of triazine is susceptible to photochemical and oxidation processes and simazine undergoes UV and visible light degradation with a very slow efficiency.[35] Thus advanced oxidation process (AOPs) have been developed to degrade triazine pollutants from water. Among AOP processes photo catalysis is as emerging technique

Simazine and atrazine degradation may follow many pathways but we focused on photolysis and photo catalysis. First process can be defined as direct when contaminant itself absorbs light and it is degraded. Indirect photolysis occurs when degradation takes place via reaction of photosensitiser molecules with pollutant(i.e. hydrogen peroxide degradation when irradiated).[26][36] Photo catalysis involves catalyst interaction with light and then with pollutant.

Since photolytic degradation alone is not able to guarantee complete mineralization, this process can be coupled with a photo catalyst to enhance process efficiency. For example, laboratory work involving TiO_2 has been done during some test with H_2O_2 that can play a role in indirect photolysis by splitting into OH radicals. Photolysis pathways described in Figure 2.5 shows The general degradation pathways of simazine, where 2-hydroxy-4,6-bis(ethylamino)-s-triazine is produced by hydrolysis (b). Photolytic loss of alkyl groups produce deisopropyl atrazine(c) and diamino chlorotriazine.(d)

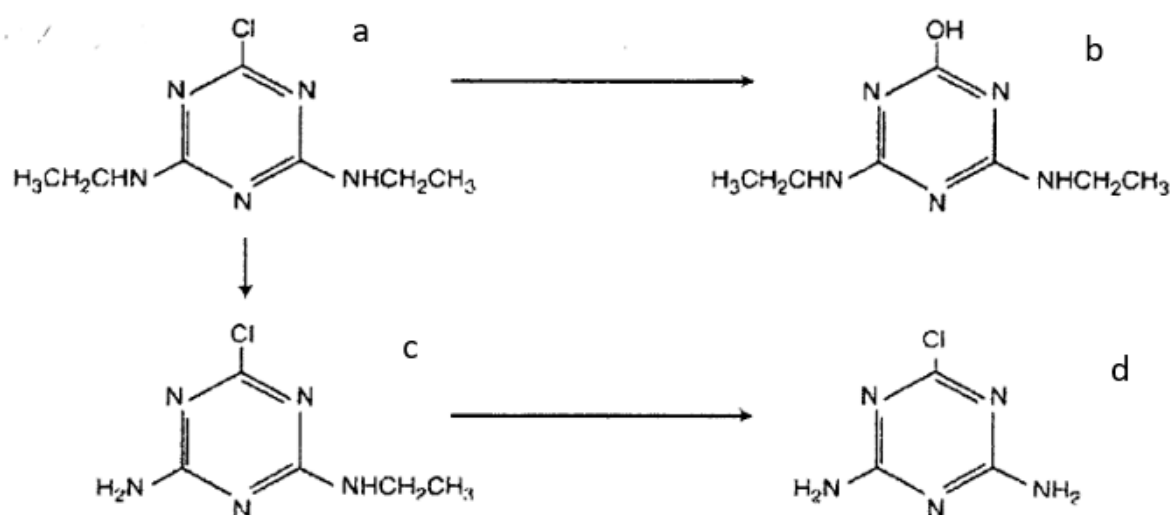


Figure 2.5 simazine degradation pathways

Indirect photolysis leads to dealkylation while hydroxylation seems to be the first step on direct photolysis reaction[35].

Indirect photolysis mechanisms of degradation are similar to photocatalytic ones because in both cases oxidation of pollutant is pursued.

Photocatalytic process leads to many intermediate molecule but the most abundant final product is cyanuric acid that have low toxicity, but ammeline and ammeline are other possible by-products. Complete mineralization of Simazine is not achieved.[27]

A possible chemistry way to degrade herbicides is high pH condition that induces dechlorination and consequently hydroxylation.

2.4 Fenton's like reaction

Fenton reactive system has been discovered by Fenton last century but today a significant number of investigations devoted to its applications are growing. Wastewater treatments is one of them because it has been demonstrated that Fenton's reagent is able to destroy toxic compounds in waste waters such as phenols and herbicides.[26]

Fenton reaction can take place in two configuration: homogenous systems in which no problems of interaction among phases are not observed but waste treatment can be a problem. On the other hand heterogeneous configuration allows easy separation of phases after reaction process but is influenced by its physical-chemical properties[3]

Fenton reaction involves two reagents: Fe and H₂O₂ and it can completely mineralized organic compounds and it is characterized by wide range of application and economy.

During reaction, highly reactive species are generated that oxidise even inorganic molecules in order to obtain less toxic substances.

We utilized mesoporous TiO₂ doped with Fe in order to induce reaction between Fe and H₂O₂ that produces OH radicals with strong oxidative effect on Simazine

Fe containing TiO₂ shows a reaction mechanism, that most probably follows a Fenton-like mechanism, in which Fe²⁺ and Fe³⁺ ions react with H₂O₂, as it is shown in the following equations;

- $\text{Fe}^{2+} + \text{H}_2\text{O}_2 \rightarrow \text{Fe}^{3+} + \text{OH}^- + \text{HO}\cdot$ (2.1)
- $\text{Fe}^{3+} + \text{H}_2\text{O}_2 \rightarrow \text{Fe}^{2+} + \text{H}^+ + \text{HO}^{2\cdot}$ (2.2)
- $\text{HO}\cdot + \text{H}_2\text{O}_2 \rightarrow \text{HO}^{2\cdot} + \text{H}_2\text{O}$ (2.3)
- $\text{HO}^{2\cdot} + \text{H}_2\text{O}_2 \rightarrow \text{HO}\cdot + \text{H}_2\text{O} + \text{O}_2$ (2.4)
- $\text{Simazine} + \text{HO}\cdot \rightarrow \text{degradation products}$ (2.5)

pH variation during Fenton reaction may induce changes in the process and it can turns in a Fenton like process

This reaction pathway is an attractive oxidative system for waste water treatment due to the fact that iron is very abundant and non-toxic element and H₂O₂ is easy to handle and environmentally safe.

Nevertheless, it is important to underline that hydrogen peroxide can attach aromatic rings by itself and so H₂O₂ can play a role during Simazine degradation that follows reaction



Possible mechanism of degradation for simazine after Fenton's like reaction is proposed in Fig 2.6 where most important by product are dealkylated (CEAT) and double dealkylated (CAAT) form of simazine. Cyanuric acid (OOOT) is presumably the final by product achievable with degradation mechanisms. Declorinated formulation of simazine (OEET) according to paper [31] is probably the main path followed by simazine during degradation

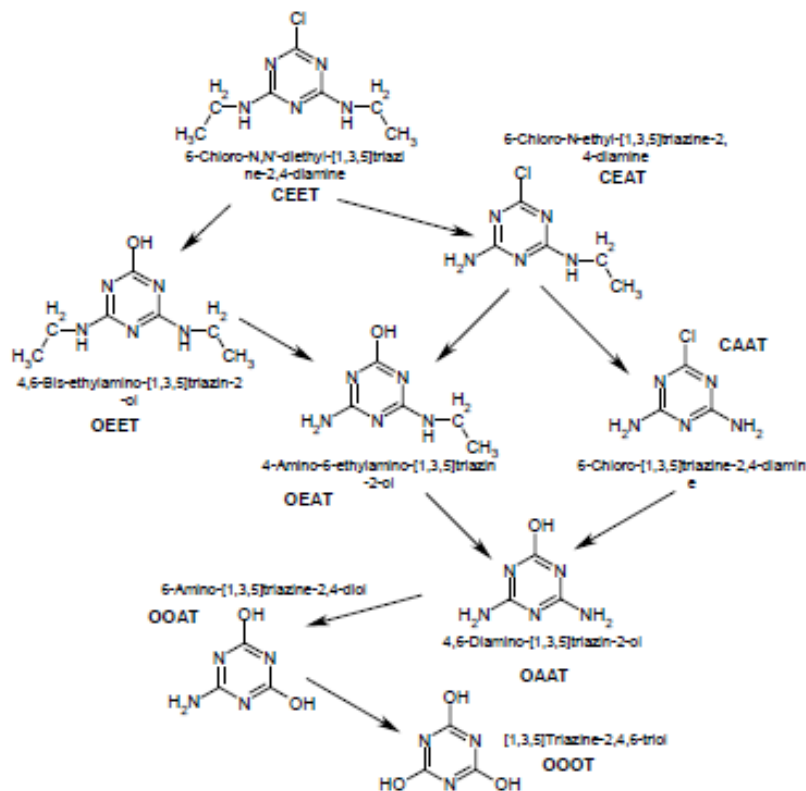


Figure 2.6 proposed mechanism for simazine degradation

3. Characterization of powders

Catalyst powders have been synthesized by following two different methods. Two different synthesis were performed, and the materials were calcined at different temperatures. In order to assess different properties in terms of

- Crystallographic structure and percentage of crystallographic phases were investigated by X-ray powder diffraction (XRD) and Rietveld refinement analysis.
- Specific Surface Area (SSA) were measured by N₂ absorption /desorption isotherms and calculated by Brunauer–Emmett–Teller (BET) model.
- Catalytic efficiency were followed by UV-vis spectroscopy.
- Energy Band Gap was calculated from diffuse reflectance UV-vis spectroscopy.
- Contamination of powders were investigated by Fourier-transform infrared spectroscopy (FTIR).
- Morphology were observed by transmission electron microscopy (TEM)

3.1 X-ray powder diffraction technique (XRPD)

This non-destructive scattering technique is used to analyse and study crystallographic structure of materials, to determine the composition either qualitatively or quantitatively.

3.1.1 The instrument.

X-rays are generated by high energy electrons hurting a copper cathode tube. Emitted radiation is then filtered to separate K α radiation, which has a defined wavelength.

Optical collimation of X-Rays is physically got by divergence, anti-scatter, and receiving slits; a diffracted beam monochromator; and a proportional counter detector having a Bragg-Brentano para-focusing geometry.

Samples are composed by small amount of powder levelled on sample holder and positioned inside the instrument.

3.1.2 Theory

Diffraction can take place when wavelengths of incident radiation and reticular parameters satisfy Bragg's law (equation 3.1 and figure 3.1)

$$n\lambda = 2d \sin\theta \quad (3.1)$$

Where:

λ = Source wavelength (nm)

n= Numeric coefficient referring to the diffraction order (usually is 1)

θ = Diffraction angle

d= Reticular diameter (nm)

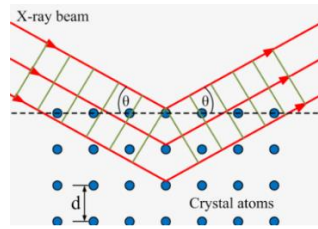


Fig 3.1 Diffraction condition

The crystallographic pattern is considered as “finger print” of every crystallographic phase. Therefore, matching the intensity and the 2θ position it is possible to obtain an analytical characterization of the sample.

3.1.3 Data acquisition

Powders have been finely grounded and then analysed with XRPD technique.

In this work XRD patterns were collected on an XPert Philips diffractometer in the 2θ angle range 10° - 90° , with a step width 0.02 and time per step of 6 s

3.1.4 Results

Fig 3.2 shows an example of two spectra detected with XRPD spectroscopy for mesoporous titanium oxide with different temperature of calcination, 700°C (blue line) and 900°C (red line).

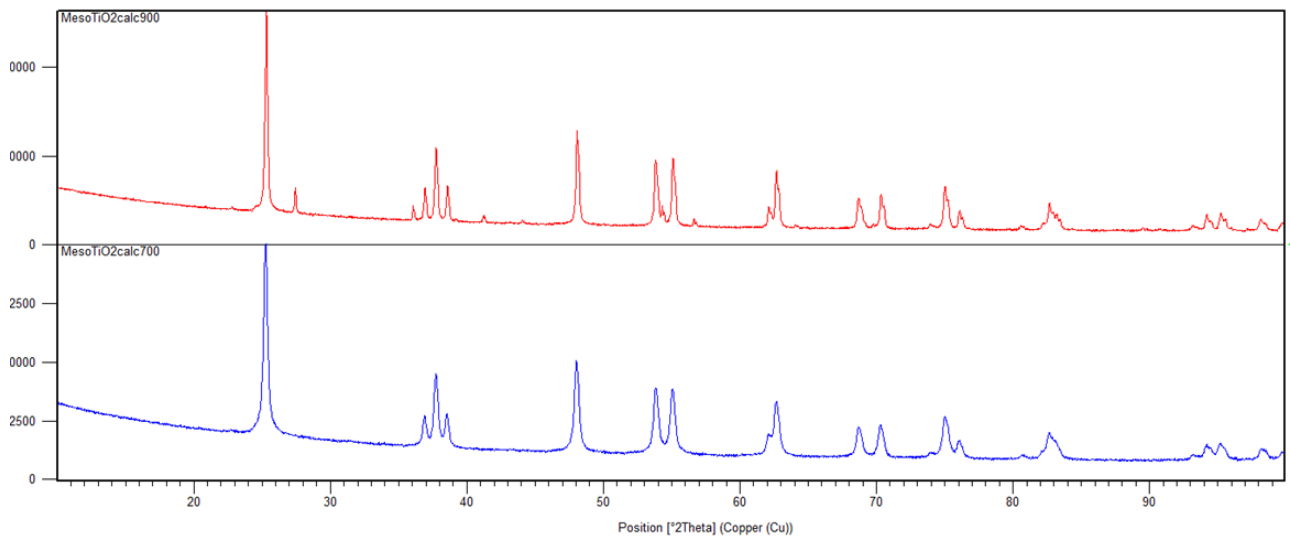


Figure 3.2 XRD spectra of Mesoporous Titania calcined at 900°C (above) and 700°C (below)

3.2 Adsorption-Desorption isotherms of N_2 at 77 K (BET)

Adsorption can be described in its common meaning as the retention of one chemical species by some of the active points in the surface of a solid. That definition limits the phenomenon to the surface, which separates the contact phases. The term adsorption is utilized in its general way to define separation process of components from a fluid phase (liquid or gas), which to the surface of an adsorbent solid. [37]

Adsorption on porous systems can be described by isotherms, reporting adsorbate amount as a function of pressure (p) divided for vapour pressure (p_0) at constant temperature.

Adsorption-desorption N_2 at 77K isotherms are valuable information to obtain several information about the surface area and pore size and distribution of a nanomaterial.

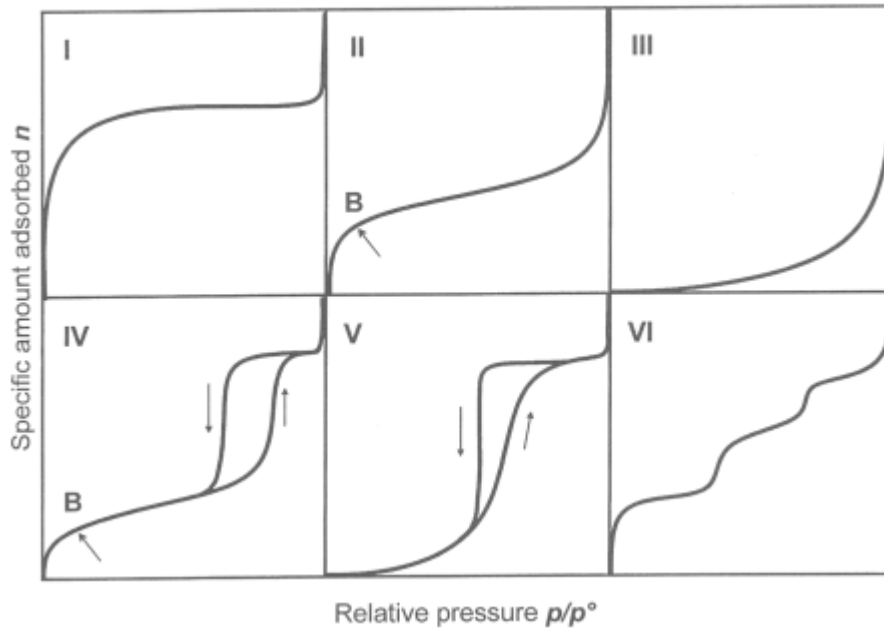
IUPAC theory for porous materials divides materials into three categories:[38]

- Nano-porous materials with pores widths below 2 nm
- Mesoporous materials with pores widths between 2 and 50 nm.
- Microporous materials with pore widths above 50 nm

According to IUPAC standard from isotherms shape is possible to understand pores shape and dimension as explained in following list

- Type I: It is microporous adsorbent (monolayer adsorption) with small external surfaces. Common one.
- Type II : this is typical for a multi-layer adsorption on microporous adsorbents with strong adsorbate-adsorbent interactions
- Type III It explains the formation of multilayer and characterizes adsorption on microporous adsorbents with weak adsorbate-adsorbent interactions.
- Type IV: At low pressure, the region of the graph is similar to Type II, explaining the formation of monolayer followed by multilayer. The saturation level is commonly reached at a pressure below the saturation vapour pressure .This can be explained according to Kelvin's law that underlines the possibility of gases condensation in the tiny capillary pores of adsorbent at pressure below the saturation pressure of the gas. Common one.
- Type V: Similar to type III with hysteresis, indicating a weak interaction between adsorbate and adsorbent. The pores are in the mesoporous range, and it is considered as a rare isotherm.

Isotherms described before are proposed in Fig 3.3[38]



3.3 Adsorption Isotherm

The Langmuir model describes systems in which, only a monolayer is formed and adsorption only occurs on localized sites on the adsorbent, no interaction between adsorbate species. Langmuir model application is Type I isotherm (*Figure 3.2*). [39] Other assumption for Langmuir model are:

- The surface containing the adsorbing sites is a perfectly flat plane.
- The adsorbing gas adsorbs into an immobile state.
- All sites are equivalent.
- Each site can hold at most one molecule (monolayer coverage only).
- There are no interactions between adsorbate molecules on adjacent sites.

In 1938, the Brunauer-Emmett-Teller (BET) theory provided theoretical support to experimental results where multi-layer adsorption occur. The BET theory is based on an simplified model of physisorption .BET theory propose that molecules in the first layer act as adsorption sites for molecules in the second layer and so on for third layer etc. [39] [40]

3.2.1 Results

In general, our samples have shown an isotherm ascribed to type IV

BET SSA is calculated by application of BET method. To apply BET method two steps are involved: First, it is important to transform a physisorption isotherm into the ‘BET plot’:[38]is important to express linear expression of BET equation(eq 3.2)

$$\frac{p/p_0}{n(1-\frac{p}{p_0})} = \frac{1}{n_m c} + \frac{c-1}{n_m c} (p/p_0) \quad (3.2)$$

Where

n is the specific amount adsorbed at the relative pressure p/p°

n_m is the specific monolayer capacity

C parameter referred to isotherm shape (if it is around 80 it is easy to understand when adsorption of multilayer starts)

Linearity range of BET plot is between 0, 05 and 0, 30 p/p_0 for type II and type IV isotherms. From linearity range of BET plot is possible to derive n_m .

BET area is derived from eq 3.3[38]

$$A(BET) = n_m \cdot L \cdot \sigma_m / m \quad (3.3)$$

Where

n_m is the specific monolayer capacity

σ_m is molecular cross sectional area of adsorbate

m is adsorbate mass

L is Avogadro number

From the knowledge of gas introduced inside samples holder is possible to know molecular cross sectional area of adsorbate.

To evaluate the pore size and distribution we applied a BJH (Barrett, Joyner, and Halenda) model on the desorption branch of the isotherm.

3.3 Catalytic properties

Catalytic properties have been investigated with ultraviolet and visible (UV-Vis) spectroscopy that is a quantitative and qualitative analysis for either organic or inorganic systems.

Visible light region is between 400 and 700 nm while UV spectrum is between 100 and 400 nm. Fig 3.4 shows schematically solar light spectrum in the UV-vis range.

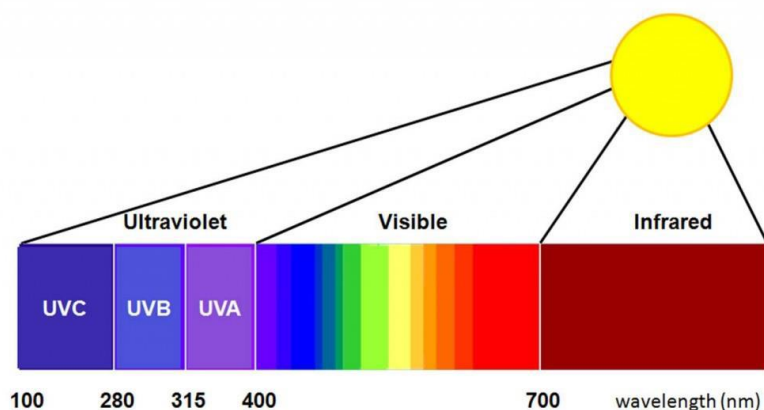


Figure 3.4 UV-vis solar light spectrum.

3.3.1 Theory

UV-vis spectroscopy is based on absorption or reflectance of light in the UV-vis spectrum range from materials. In this range, molecules and atoms can undergo electronic transitions, for example in molecules can involve transitions between HOMO and LUMO levels. Each molecule has its own absorption spectrum as long as molecular orbitals structure is peculiar of each molecules.

Fig 3.5 shows schematically the basic structure of a spectrophotometer.

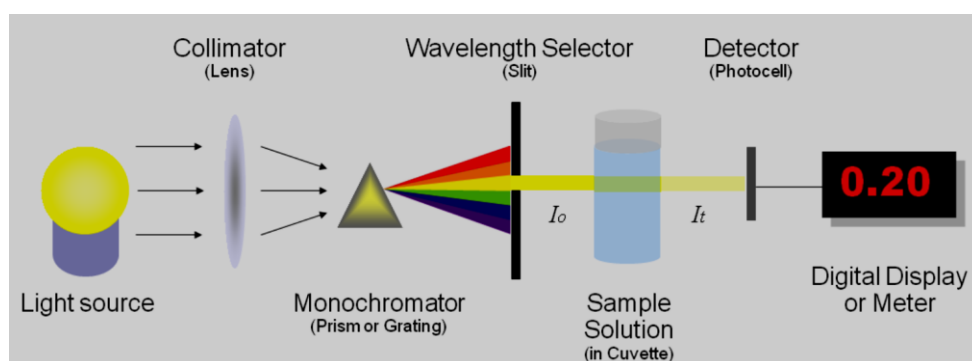


Figure 3.5 Spectroscopy scheme[41]

Intensity of light decreases exponentially as it passes through an adsorbing medium. Absorption, (A) is defined as:

$$A = \log\left(\frac{I}{I_0}\right) \quad (3.4)$$

Where:

I_0 is the intensity of the incident light. [cd]

I is the intensity of transmitted light [cd]

Lambert Beer law (eq3.5) quantifies adsorption process at a given wavelength:

$$A = \epsilon Cl \quad (3.5)$$

Where

ϵ is Molar Extinction Coefficient that is constant for absorbing species and defines absorption at a specific wavelength. It is determined by molecular orbitals in molecules.

C is concentration of solution in the cuvette. [mole/L]

l is length of the path of light through solution. [mm]

3.3.2 Procedures

We utilized UV-Vis spectroscopy in order to follow catalytic processes. Solution containing simazine with photocatalytic powders has been prepared and irradiated with solar lamp. Solution has been centrifuged to let powders precipitate and then simazine spectrum has been recorded after constant interval of time of irradiation (1h (dark condition) then 60 minute(min) 120 min, 180 min, 240 min ..).

3.3.3 Results

Fig 3.6 shows simazine UV-Vis spectroscopy spectrum

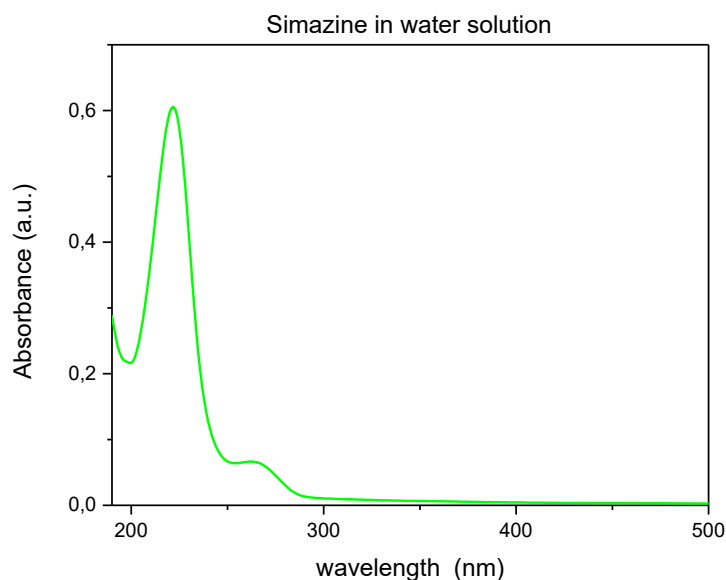


Figure 3.6 Simazine in water solution

Simazine spectrum can be divided in three areas:

- An area around 200 nm of wavelength.
- One peak at 221 nm due to aromatic part of simazine molecule ($\pi \rightarrow \pi^*$).
- One smaller peak at 270 nm related with later chain of simazine molecule ($n \rightarrow \pi^*$).

3.4 Transmission electron microscopy (TEM)

Morphological properties of powders have been studied with transmission electron microscopy (TEM) in order to evaluate porosity and nanoparticles dimensions and porosity, which can be intercrystallites or intracrystallites depending on synthesis methods.

3.4.1 Theory

TEM is an imaging technique based on electrons beam focusing through different series of electromagnetic lens onto a specimen. At the end an enlarged version of the sample is projected on a fluorescent screen or layer of photographic film[42].

Electrons microscopy has some advantage compared to light microscopy. Thanks electron beam, which has smaller wavelength compared to light it, is possible to observe nanomaterials with higher resolution. According to Rayleigh's scattering criterion (eq3.6) smallest distance that can be resolved follows:

$$\delta = \frac{0,61\lambda}{\mu \sin\beta} \quad (3.6)$$

Where

δ smallest distance that can be resolved [nm]

λ wavelength of the radiation [nm]

μ the refractive index

β is semi-angle of collection of the magnifying lens.

Eq 3.6 explains that light microscopy can have a maximum resolution around 300nm while TEM microscopy can go well below this resolution; so far, it is 0.05 nm. According to equation 3.5 that correlates energy(with wavelength of electrons, considering De Broglie studies, it is possible to understand quantitatively resolution achievable with electron microscopy when relativistic effects are ignored [43]

$$\lambda = \frac{1,22}{E^{1/2}} \quad (3.7)$$

Where

E eV)

λ wavelength (nm)

Electrons beams interact with matter in different ways as Fig 3.7 shows

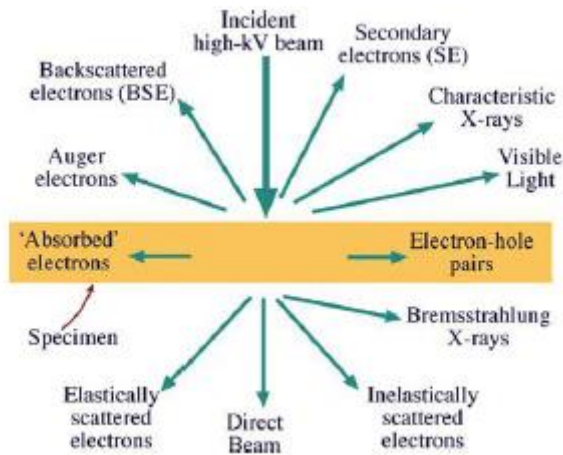


Figure 3.7 Signals generated when high voltage electron beams interact with specimen[43]

Different types of TEM can detect most of the signals.

Electrons are focused with electromagnetic lenses and limiting apertures in order to focus an electron beam of few micrometers .[43]

Crystallites dimensions have been measured.

3.4.2 Procedure

The powder was dispersed in water and briefly sonicated. Then a drop of the suspension was deposited on small grid supported by carbon film. Grid diameters is 3 mm. Fig 3.8 shows sample holder for TEM analysis.



Figure 3.8 Sample Holder TEM [44]

We used a FEI Tecnai TEM, which guarantees a resolution of 2.04 Å (lattice) and 3.5 Å (point to point) at 120 kV

Fig 3.9 shows the picture of FEI tecnai TEM



Figure 3.9 FEI Tecnai TEM

3.5 Infrared spectroscopy (IR)

Infrared spectroscopy is suitable to evaluate interaction between matter and electromagnetic radiation with wavenumber between 12800 and 10 cm^{-1} while common range of analysis is between 4000 cm^{-1} and 400 cm^{-1} . Across this region is possible to define three regions:

- 4000-1300 cm^{-1} called functional group region where most of signal referring to functional group can be detected.
- 1300-600 cm^{-1} called finger printing region where bands detected are unique to each molecule.
- 650-200 cm^{-1} called far IR region where bands due to heavy atoms and heavy molecular structure can be observed.

Where wavenumber is defined as:

$$\bar{\nu} = \frac{\nu}{(c/n)} \quad (3.8)$$

Where

c : velocity of light in a vacuum (2.997925×10^{10} cm/sec)

n : refractive index in which the wavenumber is measured (1,0003 refractive index of air) (adimensional)

ν frequency independent of the medium and expressed in Hertz (Hz)

Frequency can be expressed like with equation 3.9

$$\nu = \frac{c}{\lambda} \quad (3.9)$$

Where λ is wavelength expressed in cm

And then wavenumber can be expressed by eq 3.10

$$\bar{\nu} = \frac{1}{\lambda} \quad (3.10)$$

Infrared spectroscopy studies vibrational and rotational frequencies of molecule. By starting from a classic model of molecules that assumes that interatomic bonding is similar to massless springs that tends to restore bond lengths and angles is possible to define $3N$ degrees of freedom for each molecule where N is the number of nuclei (atoms or ions in a molecule). Three rotational coordinates have to be specified for non-linear molecules. Rotation about the centre of gravity and translation around it of molecules do not change molecule shape. These degrees of freedom are subtracted from total degree of freedom $3N$. Hence vibrational degrees of freedom of molecules are:

- $3N - 6$ for nonlinear molecules
- $3N - 5$ for linear molecules

Every degrees of freedom correspond to an independent normal mode of vibration. Mode of vibration can be mainly divided in:

- Stretching vibration when interatomic displacement of atoms occurs along axis.
- Bending vibration when variation of angles between interatomic bonding occurs without interatomic bonding distance variation. These movements can be divided into:
 - In a plane: scissoring and rocking.
 - Out of plane: wagging and twisting.

Molecules are composed by different atoms with a proper interatomic distance. These two aspects explain why dipole moment is defined as:

$$\mu = q \cdot d \quad (3.11)$$

Where

μ is dipolar moment [esu cm]

q is electric charge [esu]

d is distance between atoms [cm]

While absorption frequency depends on molecular vibrational frequency, the absorption intensity depends on energy transfer mechanism from infrared photons to molecules. Energy transfer is due to a change in dipole moment that takes place in response of molecular vibration. Dipole moment variation would induce an electric field with consequent interaction with infrared radiation.[45]

It is important to underline that not all infrared radiation will cause a change in dipole moment and hence absorption of energy takes place just for some frequencies.

Infrared spectroscopy can be also based on Lambert-Beer law

$$A = \varepsilon \cdot c \cdot d \quad (3.12)$$

Where:

A = absorbement [adimensional]

c = concentration; [mole/L]

ε = extinction coefficient [L/moli*cm]

d = sample width. [cm]

Fourier Transform Infrared spectroscopy (FT-IR) is based on Michelson interferometer.

The instrument is based on a conventional infrared source. After interacting with the sample, infrared beam is collimated and directed to a beam splitter that generate two optical paths. In one path, a fixed position mirror reflects the beam while other ray is reflected but in this case by a movable mirror, which commonly is kept 2.5 μm backwards. The part of energy that is not reflected reaches the detector. By reaching the detector signal turns from frequencies to time domain utilizing Fourier transformation in order to reduce noise of signals.[46]

Every functional group has its peculiar vibrational frequency.

3.5.1 Transmission infrared spectroscopy

Sample has been prepared by forming a thin layer from powder. Before, powder was finely ground to have small particles to avoid scattering, which can cause a slope baseline spectrum

Sample are almost 10 μ m thick in order to guarantee no diffusion of light. Powders are inserted between gold layers and then sample are positioned inside quartz container that can withstand high temperatures and vacuum conditions for treatment before and during the analysis.

4. Synthesis and materials

Materials were prepared by following wet-chemistry methods. Two main synthesis and different temperatures of calcination were applied to tune material properties and obtain different crystallographic polymorphisms for photocatalytic processes. The two methods mainly differ from each other for the use of a soft template during the synthesis process: while the first proposed method uses a triblock copolymer, the second proposed method does not apply any template but the particle formation is based on pH changes.

4.1 Synthesis n°1: mesoporous titanium dioxide

Mesoporous titanium dioxide was produced by soft template method. Multiple calcination temperatures were utilised in order to obtain crystallographic variation of materials.

Two solutions were prepared:

- Solution A:
 - Acetic Acid 20% v/v (120ml)
 - Titanium butoxide (20g)
- Solution B
 - Pluronic P123 a triblock copolymer(12g)
 - Ethanol (80ml)

Two solutions were prepared in two different beakers and stirred for 4 hours in order to gain homogeneity. Then, the two solutions were mixed by adding solution A to solution B beaker dropwise with purpose of obtaining a milky-like solution with no aggregates.

Mixed solution were left under stirring for 24 hours at room temperature. After that, we poured the solution in a Teflon autoclave and left it in a stove at of 98°C for 48 hours.

Final solution was then washed with ethanol and bi-distilled water. Solution was then centrifuged (4000 rpm for 12 minutes) and washed again until supernatant did not show particles or aggregates. Eventually, the obtained powder was dried inside stove at 60°C.

The synthesized powders were calcined at different temperatures. T was raised at 1.8° C/min up to T of calcination, and then the sample was calcinated for 4h at 700°C or 900 °C (depending on which sample) before cooling down at 1.8 °C/min and the samples were labelled as following

- 700 °C (MesTiO₂700)
- 900°C(MesTiO₂900)
- 450°C(MesTiO₂_450)

4.1.1 Direct method with Fe (MesTiO₂dirFe)

To decrease the band gap of mesoporous titanium dioxide and to absorb more photons in the visible range, we doped the material by introducing directly during the synthesis a precursor of iron.

Therefore, the only variation to synthesis number one was the addition of 2.5 g of inside solution A. The other synthesis steps were kept the same and calcination temperature utilised was 450°C. At the end, we obtained a mesoporous titania doped at 2.5% wt with iron, directly present in the TiO₂ lattice.

4.2 Synthesis n°2: brookite synthesis

This synthesis method developed by Mutuma et al [47] is proposed with the aim to obtain materials composed by a mixture of different TiO₂ crystal polymorphs. Synthesis method can be described as modified sol-gel method with no template usage.

Chemicals utilized were:

- Titanium(IV)isopropoxide(TTIP)
- Isopropyl alcohol, C₃H₈O
- Nitric acid, HNO₃
- Bi-distilled water, H₂O

Synthesis process can be briefly summarized as follow: 30 ml of TTIP was mixed with 30 ml of isopropyl alcohol and stirred (500 rpm) for 20 min in 150 ml beaker. Bi distilled- water (300 mL) was added to the mixture under vigorous stirring. After mixing period the solution was heated to 80 °C in a stove for 5 h and then cooled to room temperature. Solution was dark yellow coloured.

After cooling, pH of the solution was controlled through addition of 1 M HNO₃ to obtain sols at pH 2. The sol was left to gel at room temperature (25 °C) under stirring for 20 hours. Obtained gel was washed with distilled water and centrifuged for 12 minutes at 4000 rpm.

Finally, gel was dried in a teflon autoclave at 100 °C for 12 h inside a stove.

Samples were calcined at T was raised at 5 °C/min up to T of calcination, and then the sample was calcinated for 2h at 200°C or 600 °C(depending on which sample) before cooling down at 5 °C/min and the samples were labelled as following :

- 200 °C in following chapters named (B1_200)
- 600 °C (B1_600)
- 200°C and then 600°C (B1_200_600)

4.3 Materials and characterization results

Catalytic powders were studied with X-ray powder diffraction, N₂ adsorption/desorption isotherm measurements. Transmission electron microscopy and DR-UV-Vis analysis.

Every sample analysis have as term of comparison a commercial TiO₂ Degussa P25, which contains a 75% of anatase and a 25% of rutile. It is characterized for low-porosity, with a specific surface area of 50 m²/g, and an average particle size of 20 nm.[48]

4.3.1 Mesoporous titanium dioxide calcined at 450°C (MesTiO₂_450)

Synthesis method is described in paragraph 4.1

XRD spectrum compared with standard XRD spectrum for anatase #01-084-1285 is proposed below (fig 4.1). It is possible to notice presence of anatase peaks (main peaks positions 25.27° and 48.01° 2θ).

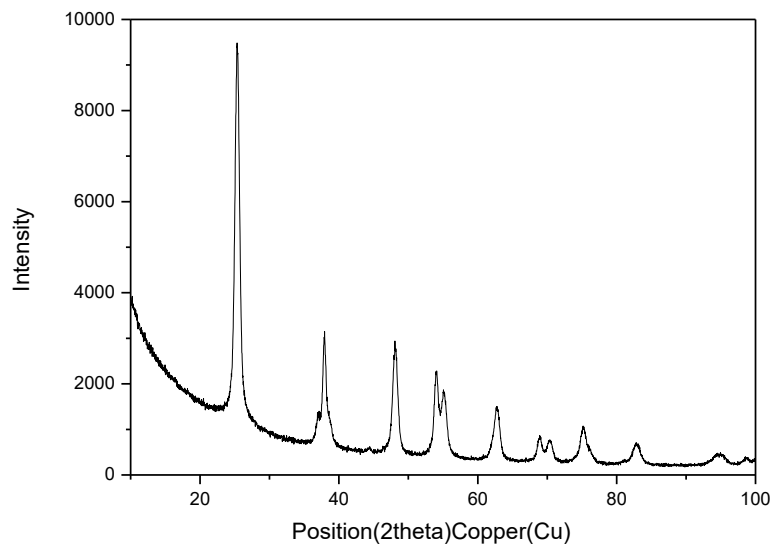


Figure 4.1 MesTiO₂_450 XRD spectrum[48]

N₂ adsorption/desorption isotherms are reported in Figure 4.2[48]

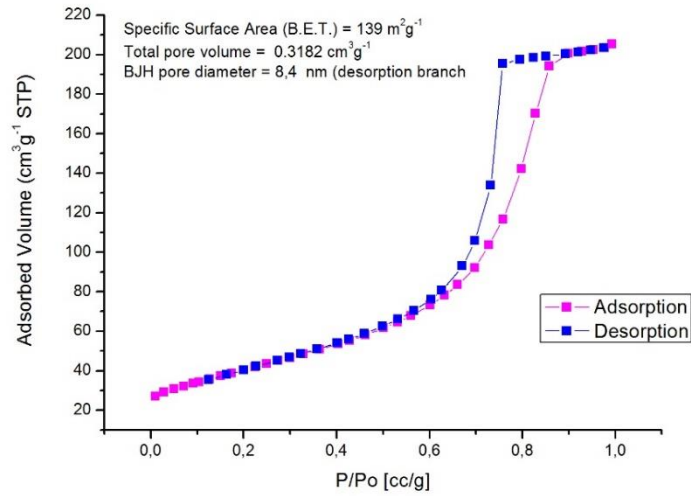


Figure 4.2 MesTiO₂_450 adsorption- desorption isotherms[48]

Fig 4.2 shows hysteresis loop typical of mesoporous materials. Loop shape suggests complex pores structure network with large pores size distribution. Desorption path (dark red) is dependent on pore blocking. This phenomenon occurs when large pores have access to external surface just through narrow necks. [38]

Table 4.1 resume schematically analysis results, we summarized BET specific surface area and BJH pore size distribution mean value based on desorption curve.

Table 4.1 MesTiO₂_450 isotherm data

Sample	BET specific surface area (m ² /g)	BJH desorption mean pore value(nm)
MesTiO ₂ _450	139	9

Fig 4.3 shows a TEM image of MesTiO₂_450

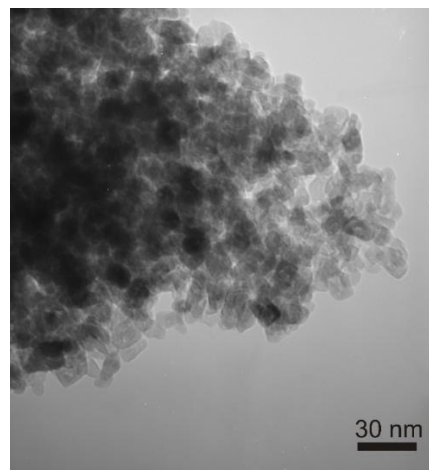


Figure 4.3 TEM image MesTiO₂_450

4.3.2 Mesoporous titanium dioxide calcined at 700°C (MesTiO₂_700)

Synthesis method is described in paragraph 4.1

XRD spectrum compared with standard XRD spectrum for anatase #01-084-1285 is proposed below (fig 4.4). It is possible to notice presence of anatase peaks (main peaks positions 25.27° and 48.01° 2θ)

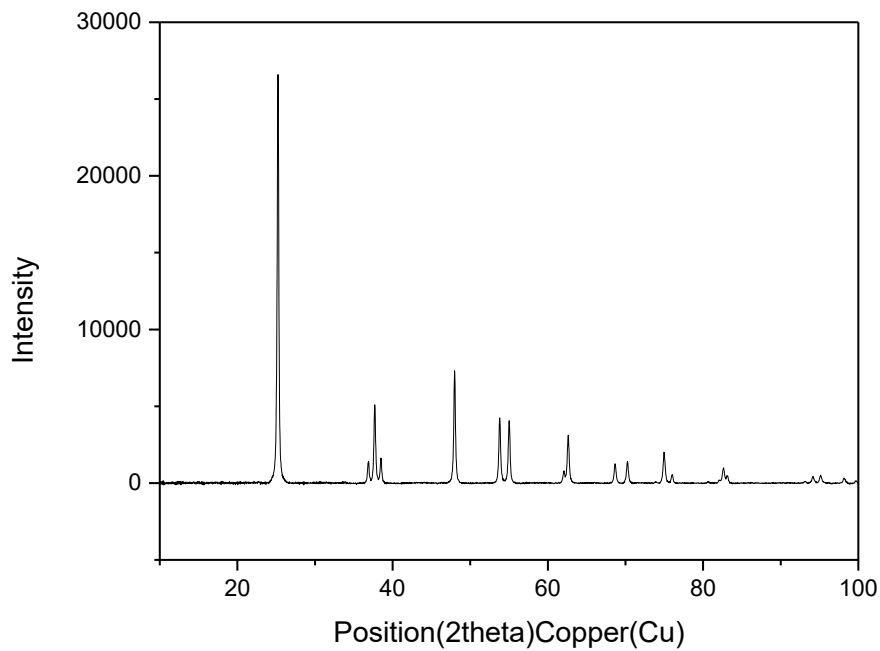


Figure 4.4 XRPD MesTiO₂_700

BET analysis spectra N₂ adsorption/desorption isotherms are reported in Figure 4.5 and had the purpose of investigating morphological properties of material

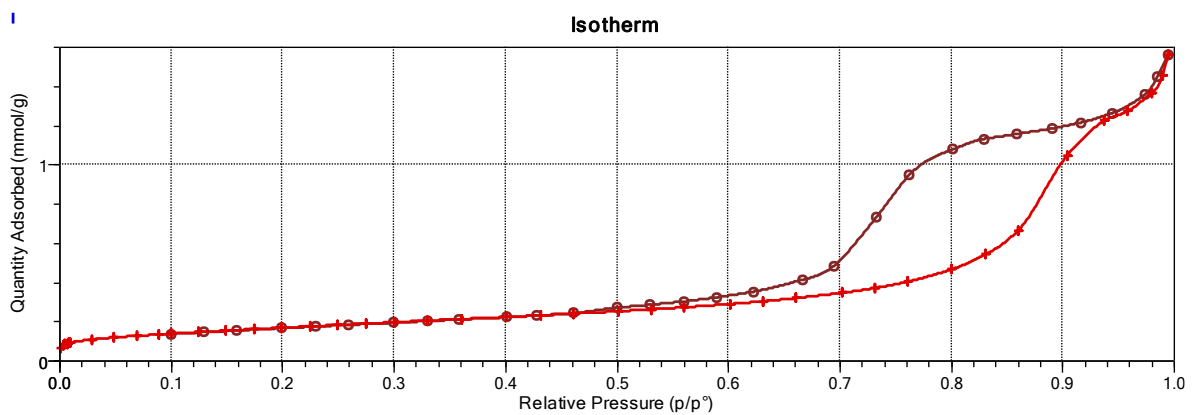


Figure 4.5 MesTiO₂_700 adsorption-desorption isotherm

Fig 4.5 shows hysteresis loop typical of mesoporous materials. Loop shape suggests complex pores structure network with large pores size distribution. Desorption path (dark red) is dependent on pore blocking. This phenomenon occurs when large pores have access to external surface just through narrow necks. [38]

Table 4.2 resume schematically analysis results, we summarized BET specific surface area and BJH pore size distribution mean value based on desorption curve.

Table 4.2 BET MesTiO₂_700

Sample	BET specific surface area (m ² /g)	BJH desorptiomean pore value(nm)
MesTiO ₂ _700	14	[7.5]

4.3.3 Mesoporous titanium dioxide calcined at 900°C (MesTiO₂_900)

Synthesis method is described in paragraph 4.1 and can be summarized as sol-gel method with soft template usage in order to obtain mesoporous material. Calcination temperature in this case was 900°C. At this temperature rutile presence has been detected.

XRD spectrum is proposed below (fig 4.6).Spectrum was compared with standard XRD spectrum #01-084-1285 for anatase and standard XRD spectrum # 96-900-4145 for rutile .In fig 4.5 it is possible to highlight presence of anatase (main peaks position 25° and 48° 2θ) and rutile peaks (main peaks position 27°, 36° and 55° 2θ)[49]

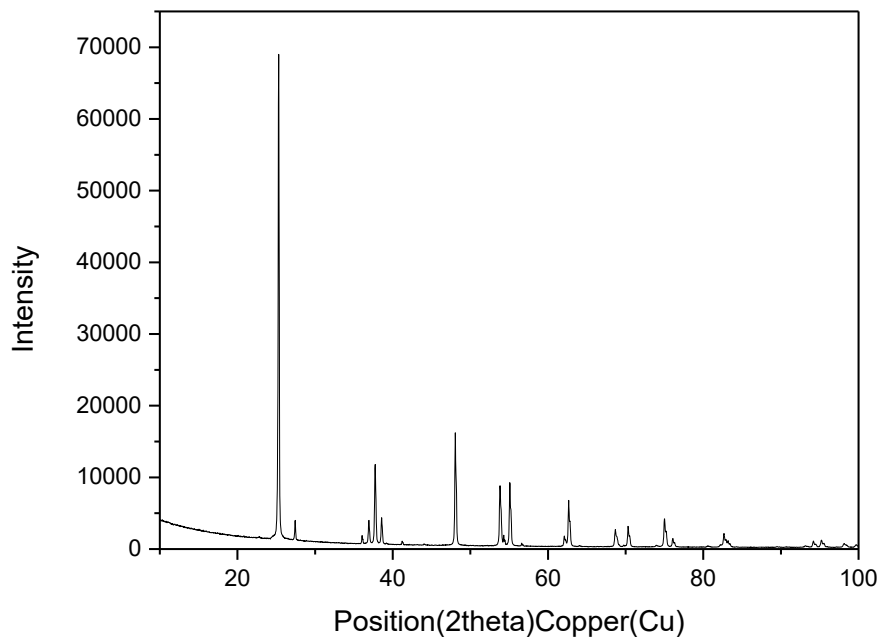


Figure 4.6 XRPD MesTiO₂_900

Fig 4.7 shows adsorption-desorption N₂ adsorption/desorption isotherms of MesTiO₂_900 sample

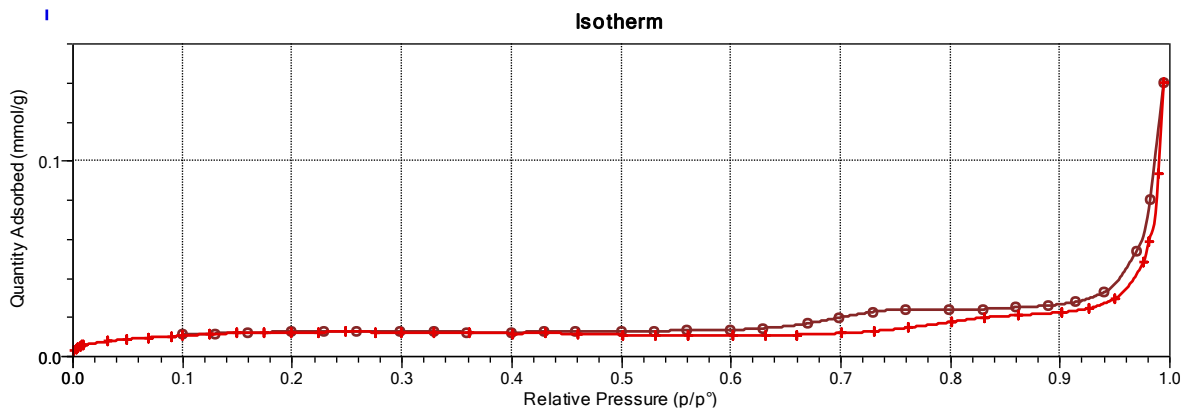


Figure 4.7 MesTiO₂_900 adsorption-desorption isotherm

Fig 4.7 shows very low porosity due to high calcination temperature. Hysteresis loop is almost absent and isotherms shape suggests macro-porous or non-porous structure.[38]

Table 4.3 resume schematically analysis results, we summarized BET specific surface area and BJH pores size distribution mean value based on desorption curve.

Table 4.3 isotherm data MesTiO₂_900

Sample	BET specific surface area (m ² /g)	BJH desorption mean pore value (nm)
MesTiO ₂ _900	1	6,3

Fig 4.8 shows TEM image of MesTiO₂_900

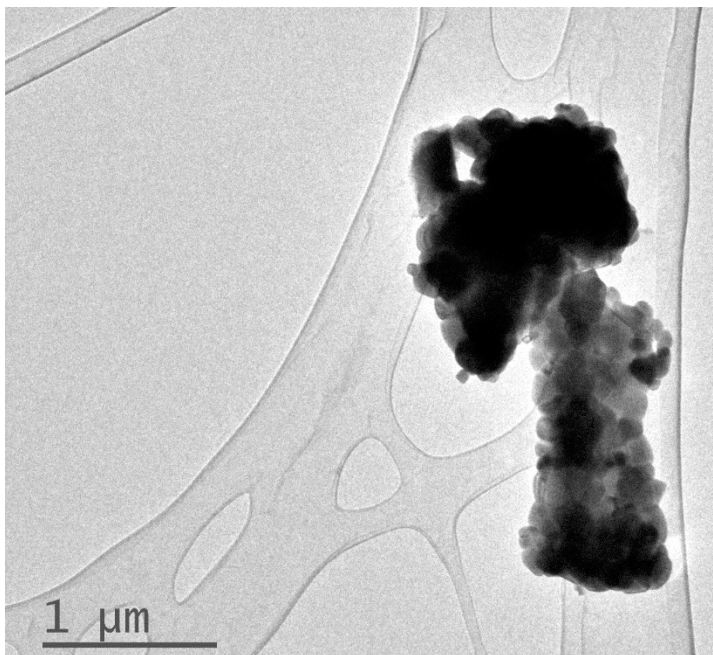


Figure 4.8 Figure 4.3 TEM image MesTiO₂_900

4.3.4 Mesoporous Titanium dioxide direct synthesis with Fe (MesTiO₂dirFe)

Synthesis method is described in paragraph 4.1 and it can be summarized as sol-gel method with soft template usage in order to obtain mesoporous material with addition of an iron precursor.

Fe precursor was added in order to obtain 2.5 wt% and calcination temperature was 450°C.

XRD spectrum is proposed below (fig 4.9) where characteristic peaks of anatase compared with standard spectrum #01-084-1285 (main peaks positions 25.27° and 48.01° 2θ) are detected. Rutile peaks compared with standard spectrum # 96-900-4145 (main peak position 27°, 36° and 55° 2θ) [49] are detected as well

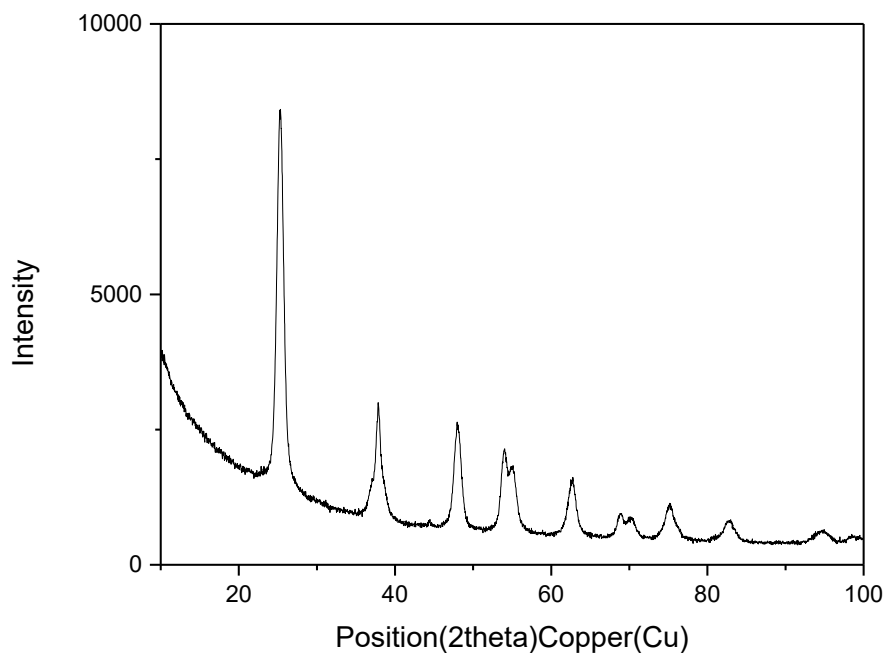


Figure 4.9 XRPD MesTiO₂dirFe

Fig 4.10 shows N₂ adsorption-desorption isotherms at 77K

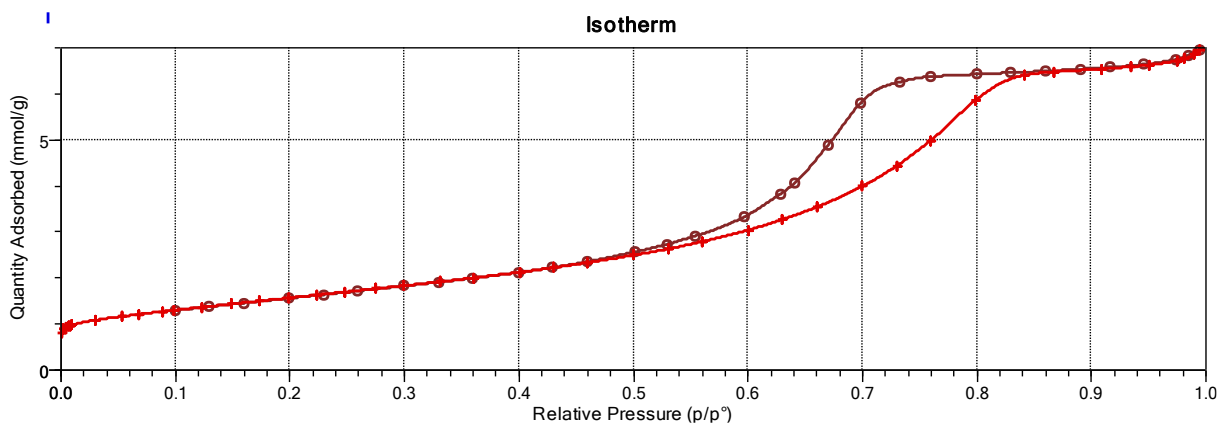


Figure 4.10 MesTiO₂dirFe adsorption-desorption isotherm

Fig 4.10 shows hysteresis typical of mesoporous materials and, by observing shape, assumptions proposed for previous samples should describe material properties.

Table 4.5 resume schematically analysis results, we summarized BET specific surface area and BJH pore size distribution mean value based on desorption curve.

Table 4.5 isotherm data MesTiO₂dirFe

<i>Sample</i>	<i>BET specific surface area (m²/g)</i>	<i>BJH desorption pore size mean value</i>
<i>MesTiO₂dirFe</i>	129	6.1

Fig 4.11 shows a TEM image of Figure 4.3 TEM image MesTiO₂dirFe

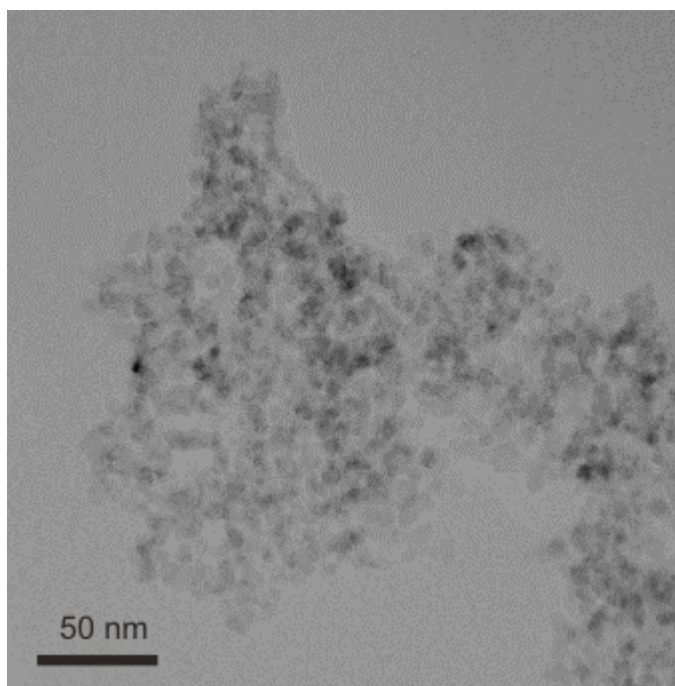


Figure 4.11 TEM image MesTiO₂dirFe

4.3.5 Second method of synthesis for titanium dioxide (B1_200)

Synthesis method described in paragraph 4.2 and it can be described as modified sol-gel method with no template usage.

Crystallographic investigation showed presence of anatase and brookite as long as high surface area due to low calcination temperature (200°C)

XRD spectrum is proposed below (fig 4.12) where characteristic peaks of anatase compared with standard spectrum #01-084-1285 (main peaks positions 25.27° and 48.01° 2θ) are detected. Rutile peaks compared with standard XRD spectrum # 96-900-4145 (main peak position 27°, 36° and 55° 2θ) [49] and brookite (main peaks at 40° and 31° 2θ) obtained from comparison with standard XRD spectrum #96-900-4139 are proposed as well).

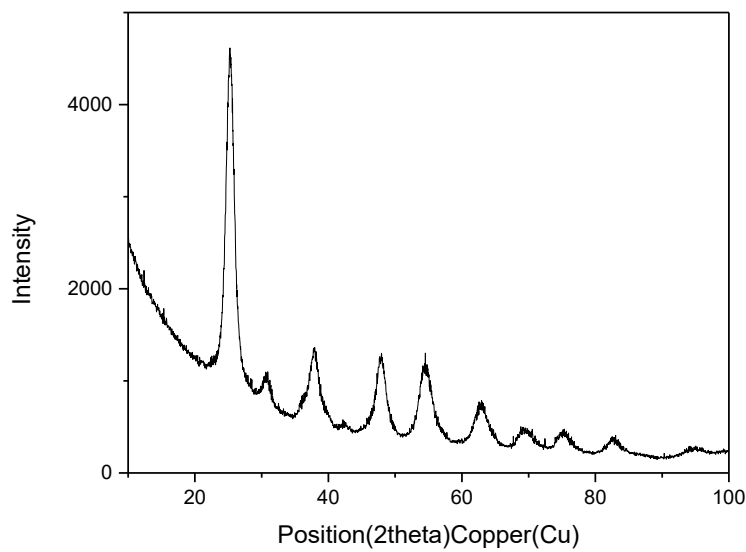


Figure 4.12 XRPD B1_200

Fig 4.13 shows N₂ adsorption-desorption isotherms of B1_200

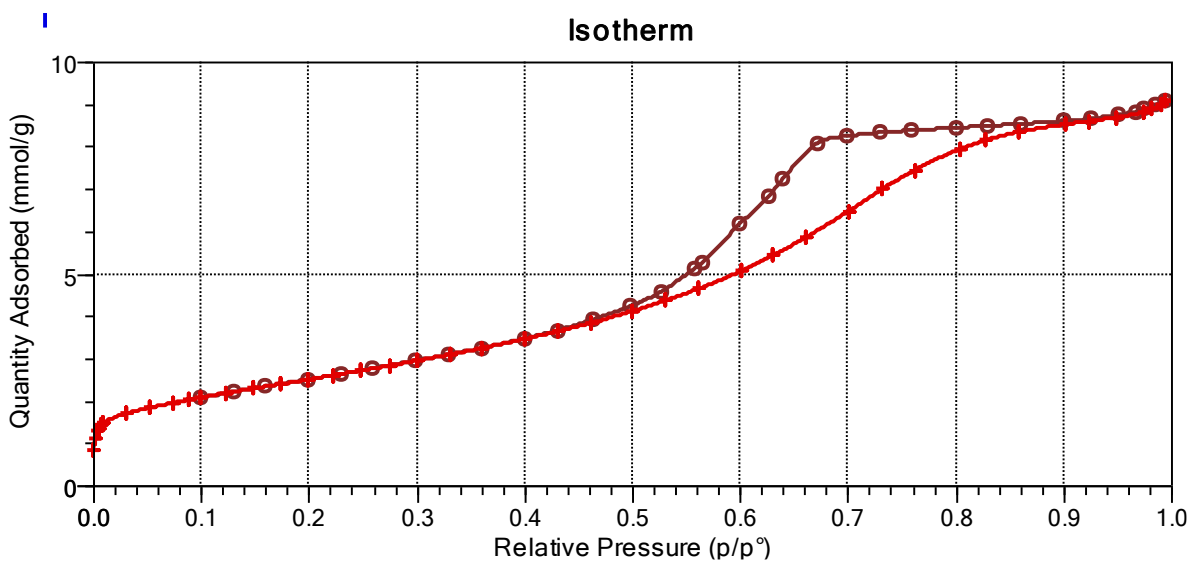


Figure 4.13 B1_200 adsorption-desorption isotherm

Fig 4.13 shows hysteresis loop typical of mesoporous materials. Loop shape is similar to MesTiO₂_700 and suggests complex pores structure network. Desorption path (dark red) is dependent on pore blocking.[38] According to Thommes et al[38]. Pore size below 5 nm may lead to cavitation induced evaporation. According to tab 4.4 pores size range should be around 5 nm.

Table 4.6 resumes schematically analysis results, we summarized BET specific surface area and BJH pores size distribution mean value based on desorption curve.

Table 4.6 isotherm data B1_200

<i>Sample</i>	<i>BET specific surface area (m²/g)</i>	<i>BJH desorption mean pore value (nm)</i>
<i>B1_200</i>	207	5

B1_200 sample showed the highest surface area compared to all samples investigated.

Fig 4.13 shows TEM image of B1_200

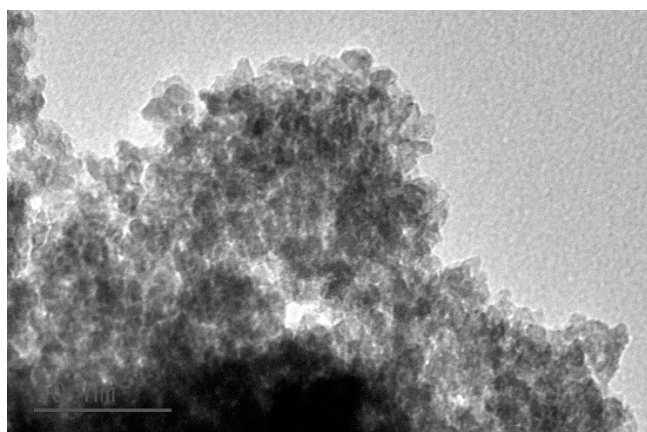


Figure 4.13 TEM image B1_200

4.3.6 Second method of synthesis for titanium dioxide (B1_600)

Synthesis method described in paragraph 4.2 and it can be described as modified sol-gel method with no template usage. Crystallographic investigation showed presence of anatase brookite and rutile.

XRD spectrum is proposed below (fig 4.14) where characteristic peaks of anatase compared with standard spectrum #01-084-1285 (main peaks positions 25.27° and 48.01° 2θ) are detected. Rutile peaks compared with standard spectrum # 96-900-4145 (main peak position 27° , 36° and 55° 2θ) [49] and brookite (main peaks at 40° and 31° 2θ) obtained from comparison with standard spectrum #96-900-4139 are detected as well.

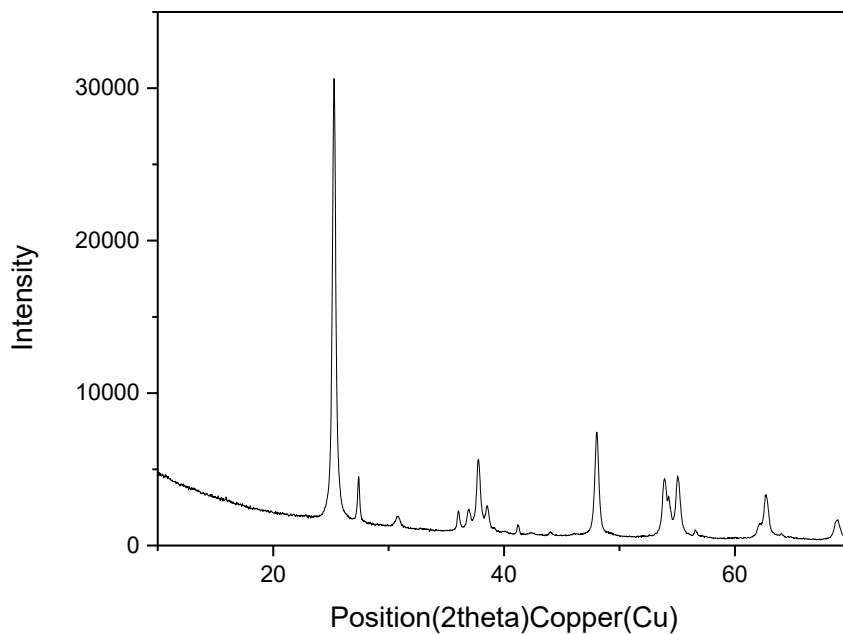


Figure 4.14 XRPD B1_600

Fig 4.15 N₂ shows adsorption-desorption isotherms of B1_600

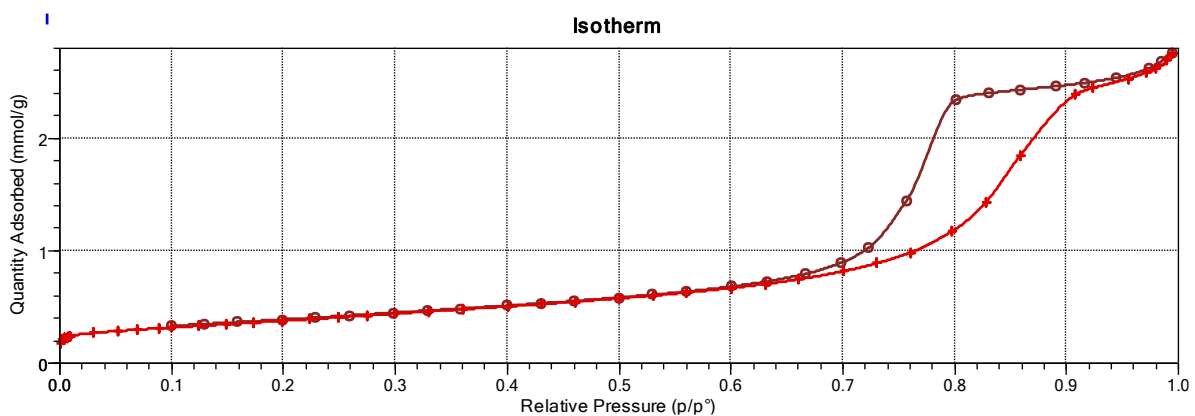


Figure 4.15 B1_600 adsorption-desorption isotherm

Fig 4.15 shows hysteresis loop typical of mesoporous materials. Loop shape suggests complex pores structure network with large pore size distribution like MesTiO₂_700 sample. Desorption path (dark red) is dependent on pore blocking. [38]

Table 4.7 resume schematically analysis results, we summarized BET specific surface area and BJH pores size distribution mean value based on desorption curve.

Table 4.7 isotherm data B1_600

<i>Sample</i>	<i>BET specific surface area (m²/g)</i>	<i>BJH desorption mean pore value (nm)</i>
<i>B1_600</i>	31	9

B1_600 sample compared with B1_200 shows lower specific surface area (SSA) probably because of higher temperature of calcination.

4.3.7 Second method of synthesis for titanium dioxide (B1_200_600)

Synthesis method is described in paragraph 4.2 and can be summarized as modified sol-gel method with no template usage. Calcination process took place in two steps: 2h at 200°C and then 2h at 600°C. Crystallographic investigation showed presence of anatase brookite and rutile.

XRD spectrum is proposed below (fig 4.16) where characteristic peaks of anatase compared with standard spectrum #01-084-1285 (main peaks positions 25.27° and 48.01° 2θ) are detected. Rutile peaks compared with standard spectrum # 96-900-4145 (main peak position 27°, 36° and 55° 2θ) [49] and brookite (main peaks at 40° and 31° 2θ) obtained from comparison with standard spectrum #96-900-4139 are proposed as well .

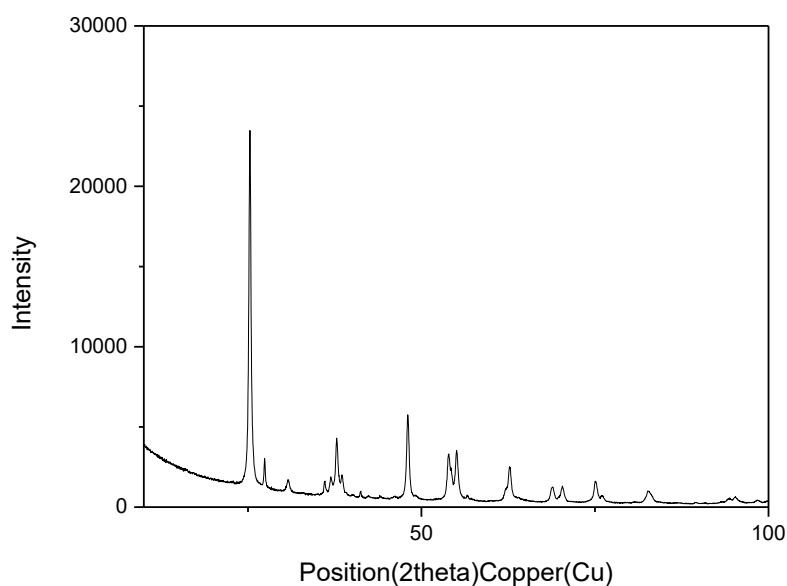


Figure 4.16 XRPD B1_200_600

Fig 4.17 shows adsorption-desorption isotherm

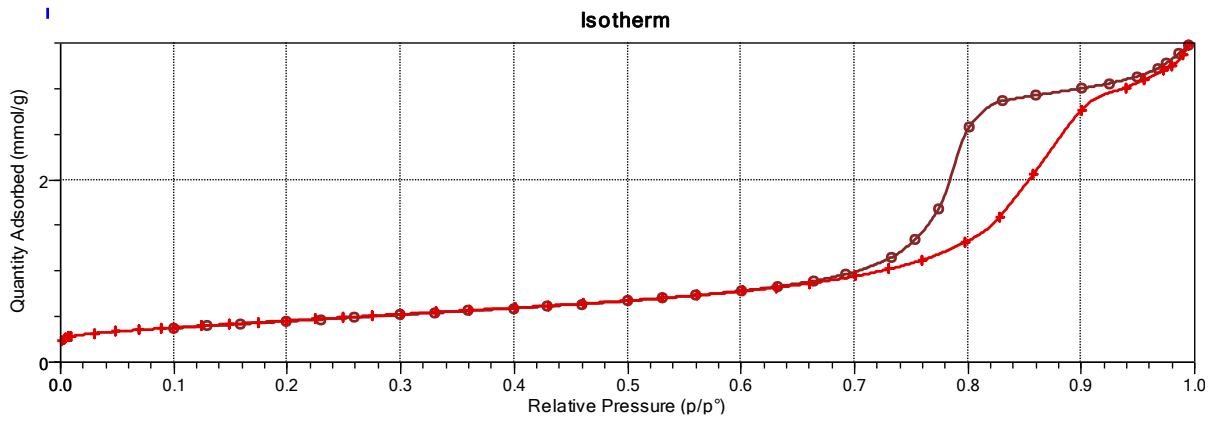


Figure 4.17 B1_200_600 adsorption-desorption isotherm

Fig 4.17 shows hysteresis typical of mesoporous materials with a large pore size distribution.

Table 4.8 resumes schematically analysis results, we summarized BET specific surface area and maximum of BJH pore size distribution when desorption branch is analysed and where pore volume distribution can be related with pore width.

Table 4.8 isotherm data B1_200_600

Sample	BET specific surface area (m^2/g)	BJH desorption mean pore value (nm)
B1_200_600	37	10

Fig 4.18 shows TEM image of B1_200_600

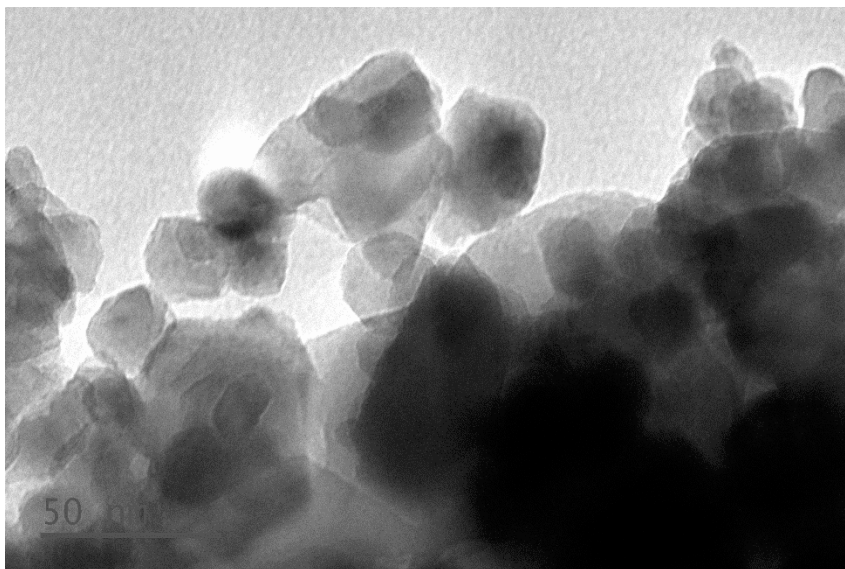


Figure 4.18 TEM image B1_200_600

4.5. Quantitative material analysis results

XRD spectra were analysed with Rietveld method in order to obtain quantitative results about crystallographic phase weight percentage of synthesized samples.

Powders were analysed by DR-UV-Vis spectroscopy and by utilizing Ewald's sphere construction and Kubelka Munk's theory and Tauc's model we calculated the band gap.

4.5.1 Rietveld analysis results

XRPD patterns obtained as described in paragraph 3.1 were analysed by Rietveld method through X-Pert Highscore software and the quantitative analysis results are reported in tab 4.9

Table 4.9 Rietveld results, obtained with XPert software

Sample	BI_200	BI_200_600	BI_600	MesTiO ₂ _700	MesTiO ₂ _900	P25	MesTiO ₂ _450
anatase	77%	84,60%	82,10%	100%	95,9%	81%	100%
brookite	23%	10,50%	10,40%		4,10%		
rutile		4,90%	7,40%			19%	

Table 4.9 Rietveld results, obtained with XPert software

P25 phases percentage derives from (Raj et al)[50] paper.

Table 4.9 shows three important aspects:

- Rutile percentage increases when calcination temperature increases.
- Synthesis method n°2 induces a mixture of different TiO₂ crystals polymorphs. Crystallographic composition is deeply different from others samples.
- Materials synthesized with synthesis method number 2-change crystallographic structure when calcined. Crystallographic phases transitions occurs while SSA decreases when sample is calcined at high temperatures.

4.5.2 Band gap investigation

Band gap results can be expressed as indirect or direct band gap.

Majority of our samples are composed by many crystallographic phases and according to Zhang et al [18] anatase appears to be direct band gap semiconductor while brookite and rutile belong to indirect band gap materials. Tab 4.10 shows energy gap of samples determined with Tauc plot model

Table 4.10 Experimentally obtained Band Gap width

Sample	Direct gap(eV)	band	Indirect gap(eV)	band
BI_200	3,11		3,44	
BI_200_600	2,97		3,11	
BI_600	3		2,52	
MesTiO ₂ _700	3,0			
MesTiO ₂ _900	3,25		3,15	
P25	3		3,64	

DR-UV-Vis spectra of samples are reported in fig 4.19

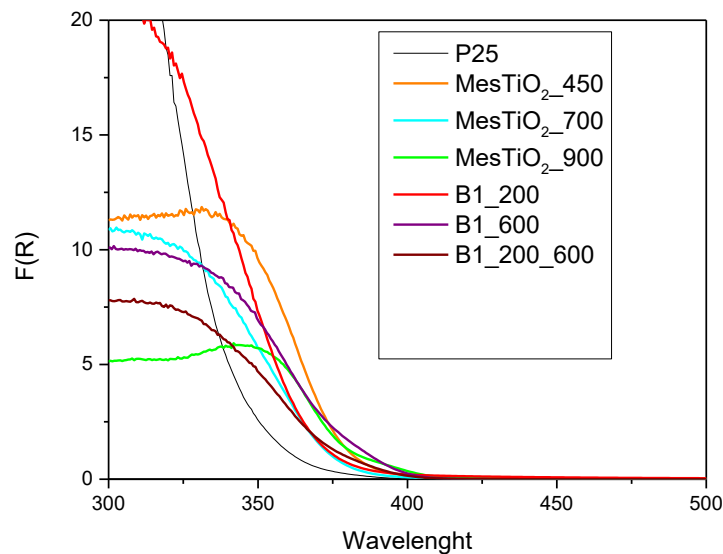


Figure 4.19 DR-UV spectra

4.5.3 Crystallites dimension investigation

TEM analysis of samples offers morphological information as long as pore presence among powders. Data reported in table 4.11 were obtained with ImageJ software. Feret diameter (d_F) is the distance between two parallel tangents to the projected outline of the particles that we obtained with transmission electron microscopy.[51]

Table 4.11 Feret diameter of samples from TEM images analysis

<i>Sample</i>	<i>Mean d_F value(nm)</i>	<i>Standard Deviation</i>
<i>B1_200</i>	7	0,8
<i>B1_200_60</i> <i>0</i>	25	3
<i>MesTiO₂_90</i> <i>0</i>	111	21

Tab 4.11 shows directly proportional correlation between high calcination temperature and crystallites size. On the other hand, synthesis n°1 is correlated with higher diameters size compared to synthesis number two.

4.6 Conclusions

Synthesis 1 based on soft template allows obtaining pure anatase phase, with high SSA, mesoporous and homogenous particle morphology and size distribution. It is possible to easily doped this kind of mesoporous material by directly adding a metal precursor during the synthesis. The calcination temperature influences the phase purity: high temperatures (above 900°C) brings to have other crystallographic phases, such as rutile but SSA sharply decreased.

Synthesis 2 based on modified sol gel method without template is suitable to obtain mixed allotropic phases structures. When calcination temperature was 200°C brookite, anatase and rutile structures were detected and sample showed very high SSA, small crystallites and pores size. With higher calcination temperature phases transitions occurred with brookite percentage decrease. SSA of materials decreases with higher calcination temperature as well.

In both cases nano organised structures are obtained and no differences were seen between MesTiO₂dirFe and meTiO₂_450 that had same temperature of calcination.

B1_200 and B1_600 samples were analysed with FTIR spectroscopy and it was discovered a certain amount of organic material on the surface of B1_200 sample that disappeared in B1_600 sample.

5. Photocatalytic tests

Photocatalytic tests were done by varying many aspects like

- catalytic powder
- catalytic concentration
- simazine concentration
- H₂O₂ concentration
- light source (UV and simulated solar light)

Every test solution was irradiated by a light source (simulated solar light lamp or UV lamp). Solutions were then centrifuged, in order to separate the photocatalytic powder from solution and then supernatant was analysed with UV-Vis spectrophotometer as described in chapter 3.3.

5.1 Experimental settings

Test conditions were varied in order either to increase simazine degradation (i.e. by utilizing H₂O₂) or to increase the grade of mimic natural environmental condition by applying simulated solar light.

Every photocatalytic tests spectra have been obtained by following same procedure:

- Simazine in water solution preparation and analysis of sampled solution with UV-Vis spectrophotometer.
- Before running the reaction under the light, the suspension was left in dark condition for 1h to reach the equilibrium between the pollutants and the photo catalyst. For this reason, the reactor (quartz tube) was wrapped in aluminium foil to isolated from room light.
- Every 60 minutes solution sample was withdrawn and then analysed with UV-Vis spectrophotometer, after centrifugation at 4000rpm for 10 minutes.

5.1.1 Catalyst

Photo-catalytic materials listed in chapter 4, were utilized during photocatalytic tests at two different concentrations 1g/l and 0,5g/l.

5.1.2 H₂O₂ usage for photocatalytic analysis.

Hydrogen peroxide was added to form OH· radicals in order to attack simazine molecules in solution through oxidation reactions. Fenton like reaction proposed in chapter 1.4.1 may suggest presence of Fe ions in solution whom interact with hydrogen peroxide. Transparent colour of supernatant during catalytic test suggested that Fe ions within the surface took part of Fenton reaction without leaching phenome.

Hydrogen peroxide was utilised above stoichiometric amount in order to push the formation of simazine:

- 6.6 time above stoichiometric amount (when simazine concentration was $5.58\text{E-}5$ M)
- 21 times above stoichiometric amount (when simazine concentration was $1.73\text{E-}5$ M)

5.1.3 Simazine concentration

Simazine solution molarity was chosen higher than EPA limits ($1\mu\text{g/L}$). We chose higher concentration compared to trace quantities present in nature to follow easier through UV-vis spectroscopy the interaction between photo catalysts and pollutants. Concentration utilized are proposed below:

- $5.58\text{E-}5$ M (solution n°1)
- $1.73\text{E-}5$ M (solution n°2)

Both solutions were obtained from mother solution by dilution.

Some tests were carried with solution n°1 to guarantee strong interaction between catalyst and pollutant. During these tests we observed solubility issues. We focused on these problems and we found solubility limit of simazine in water that according to Hayes[52] is $1.73\text{E-}5$ M. Mother solution has been diluted in order to obtain solution n°2.

Simazine solution volume for every photocatalytic tests was fixed to 50 ml.

5.1.4 Lamps and reactor

Test configuration chosen is resumed in picture 5.1 where solar light simulated lamp (on the left of the picture) is positioned at fixed distance from quartz tube (reactor). Stirrer plate is positioned below reactor in order to guarantee continuous stirring during tests.



Figure 5.1 Solar simulated lamp

Solar simulated lamp (called solar lamp) power was set in order to radiate 1 SUN of light intensity. Lamp spectrum contains small quantity of UV light.

On the other hand, some tests were done with UV lamp with configuration of 55-61 mW/cm² as defined intensity.

5.2 Blank experiments:

5.2.1 tests without catalyst.

We studied interaction between simazine and light, with and without H_2O_2 , in order to deeply understand photocatalytic reaction pathways in absence of catalyst. Concentration of simazine solution selected in both cases was $5.58E-5M$ (solution 1)

5.2.2 Simazine photolysis

Fig 5.2 shows UV-Vis spectroscopy spectra when any catalyst is present in the solution.

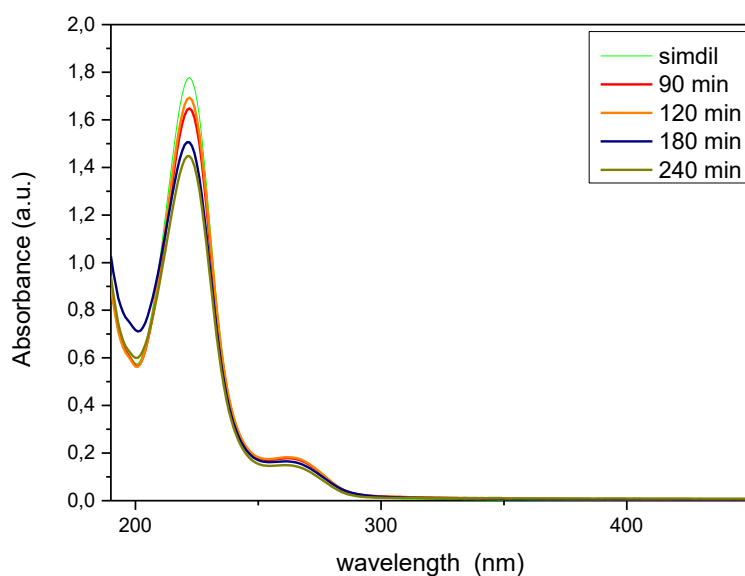


Figure 5.2 Simazine solution under solar lamp irradiation

During our tests, we discovered that simulated solar light might degrade around 19% of simazine after four hours of illumination.

We tried photo catalysis pathway in following tests in order to enforce simazine degradation due to photolysis.

5.2.3 H₂O₂ interaction with simazine

Fig 5.3 shows UV-Vis spectra of simazine and hydrogen peroxide in water solution without the presence of any catalyst

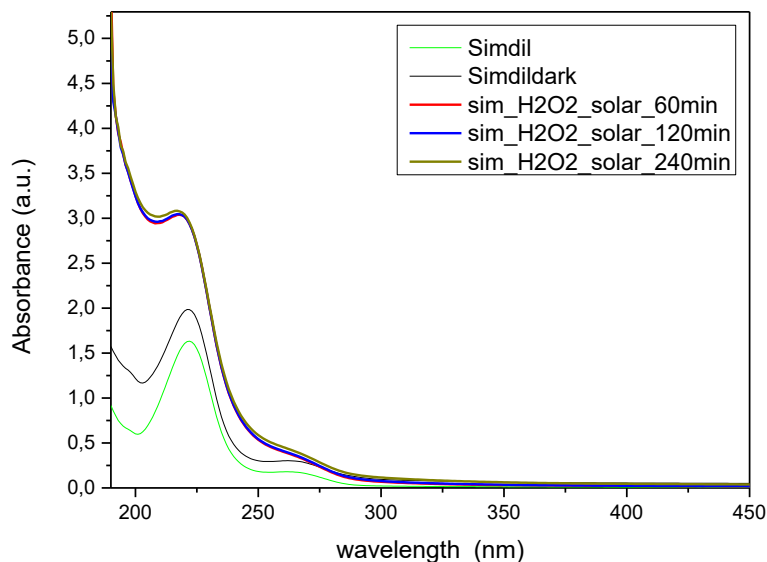


Figure 5.3 hydrogen peroxide and simazine solution, no catalyst presence

Two main aspects can be seen in fig 5.3:

- Hydrogen peroxide addition in absence of catalyst hides simazine spectrum and therefore it is more difficult to evaluate its effectiveness since no variation of peaks can be clearly noticed.
- After hydrogen peroxide addition (after one hour of dark condition), there is not any evident variation of H₂O₂ spectra under illumination.

5.3 Photo catalysis tests in presence of photo-catalytic materials.

Analysis configuration consists of simulated solar lamp and reactor with or without hydrogen peroxide. Simazine concentration was changed as well catalysts type.

5.3.1 Solution n°1 MesTiO₂_450 H₂O₂

In this experiment, we used 50 mL of simazine solution (5.58E-5 M) in presence of 1g/L of MesTiO₂_450. Aliquots of the sample were withdrawn every 60 min but here we reports only after 60 min and 240min. H₂O₂ was added after initial 60 minute in dark condition.

Fig 5.4 shows UV-Vis spectra of test regarding MesTiO₂_450 in simazine solution with hydrogen peroxide presence.

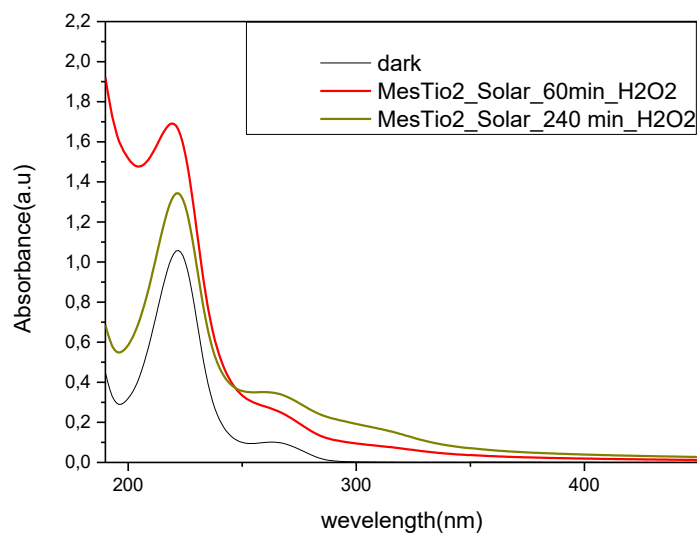


Figure 5.4 MesTiO₂_450 in simazine solution with hydrogen peroxide under solar simulated lamp

Fig5.4 spectra can be analysed as follow: red line curve (60 minutes irradiation) show a non-equilibrium condition within solution between hydrogen peroxide simazine and catalyst. Dark yellow line shows that in presence of H₂O₂ and catalyst after four hours of illumination there is a blue shift of 221 nm peak. According to (Chen et all) [33] blue shift is probably due to lateral chain loss and consequently simazine degradation. Peak emerging at 300 nm is due to nitrates generation.

5.3.2 Solution n°1 MesTiO₂dirFe H₂O₂

In this experiment, we used 50 mL of simazine solution (5.58E-5 M) in presence of 1g/L of MesTiO₂dirFe. Aliquots of the sample were withdrawn every 60 min but here we reports only after 60 min, 180 min and 240min. H₂O₂ was added after initial 60 minute in dark condition

Mesoporous MesTiO₂dirFe was tested with hydrogen peroxide presence and with simazine concentration described by solution n°1. Fig5.5 shows UV-Vis spectra

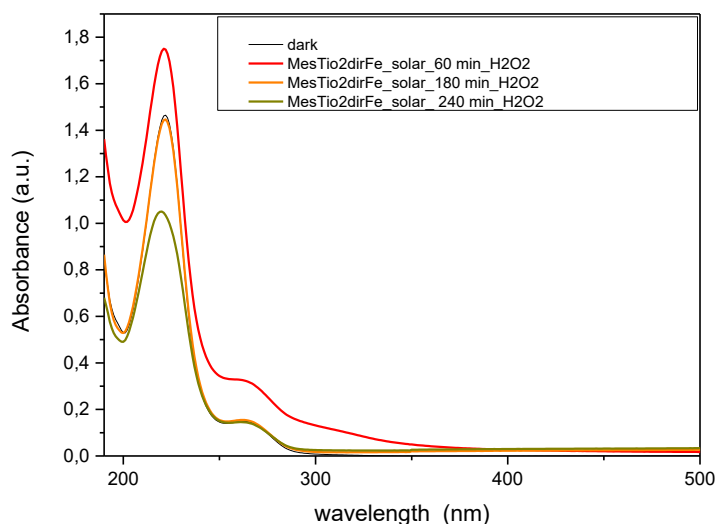


Figure 5.5 MesTiO₂dirFe in simazine solution with hydrogen peroxide presence

Fe doping has the purpose of reducing band gap and so enforces photo catalyst efficiency when light source is solar light.

Fig 5.5 shows non-equilibrium condition after 60 minutes illumination and almost there is any reaction involving hydrogen peroxide after 3 hours upon solar lamp. After four hours, a sharp decrease of 221nm peak (27%) can be observed. Small blue-shift of the peak position (through smaller wavelength) may be due to lateral chain loss.

Photocatalytic high efficiency is due to two aspects, both regards Fe presence. First possibility is Fenton reaction between Fe and hydrogen peroxide without Fe in solution. Second pathway may be simple enforce of visible light absorption due to Fe doping like previously explained.

5.3.3 Solution n°1 Degussa P25 H₂O₂

In this experiment, we used 50 mL of simazine solution (5.58E-5 M) in presence of 1g/L of Degussa P25. Aliquots of the sample were withdrawn every 60 min but here we reports only after 60 min, 180 min and 240min. H₂O₂ was added after initial 60 minute in dark condition

Fig 5.6 shows UV-Vis spectra of photocatalytic test with Degussa P25 in presence of hydrogen peroxide for simazine degradation purpose. Solution utilized is solution n°2.

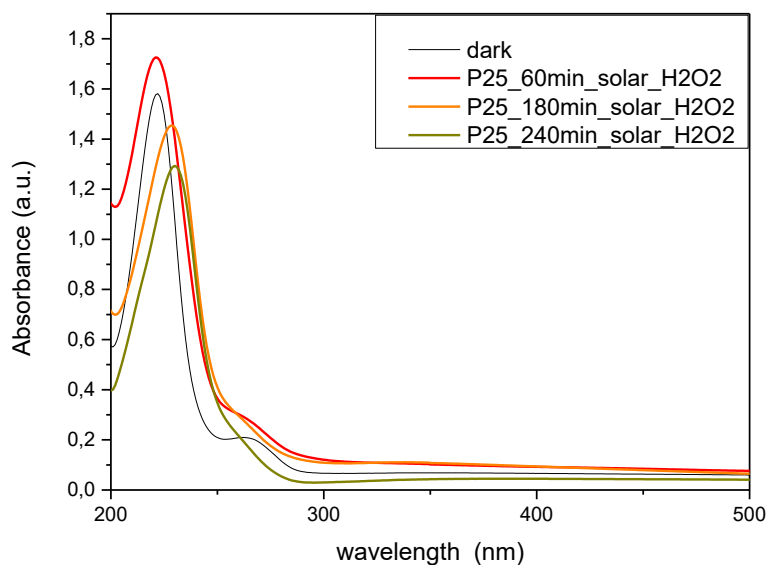


Figure 5.6 Degussa P25 in simazine solution with hydrogen peroxide presence

P25 commercial powder interacted with simazine by different pathways as long as 221 nm peak shows a red shift (through higher wavelength) of the position. Red shift is associated with dechlorination- hydroxylation reaction. At the same time, the later band (270 nm) shape clearly changes, which is not present anymore after 4 hours (dark yellow curve), probably a consequence of lateral chain loss.

5.3.4 Solution n°2 MesTiO₂_450 H₂O₂

In this experiment, we used 50 mL of simazine solution (1.73E-5 M) in presence of 1g/L of MesTiO₂_450. Aliquots of the sample were withdrawn every 60 min but here we reports only after 60 min, 180 min and 240min.

Fig 5.7 shows MesTiO₂_450 with solution n°2(1,73E-5M) without hydrogen peroxide and solar simulated lamp

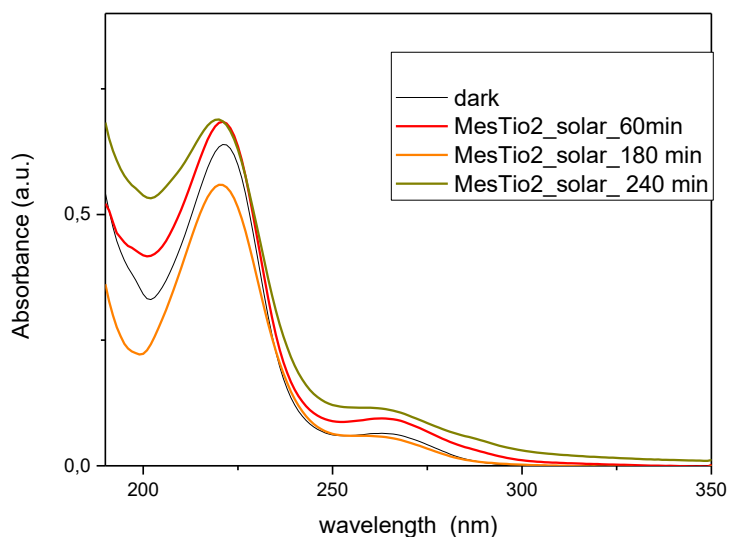


Figure 5.7 MesTiO₂_450 in simazine solution under solar simulated lamp

Fig 5.7 shows simazine degradation under not equilibrium conditions since after three hours of illumination the band at 221 nm is lower than dark yellow band (4h illumination). On the other hand, it is possible to observe some variations in the spectrum like shape changes of spectra around 200 nm and 270 nm.

5.3.5 Solution n°2 MesTiO₂_900

In this experiment, we used 50 mL of simazine solution (1.73E-5 M) in presence of 1g/L of MestiO₂_900. Aliquots of the sample were withdrawn every 60 min and all of them are reported in the spectra.

Fig 5.8 shows UV-Vis spectra of MesTiO₂_900 samples dispersed in solution n°2 with solar illumination.

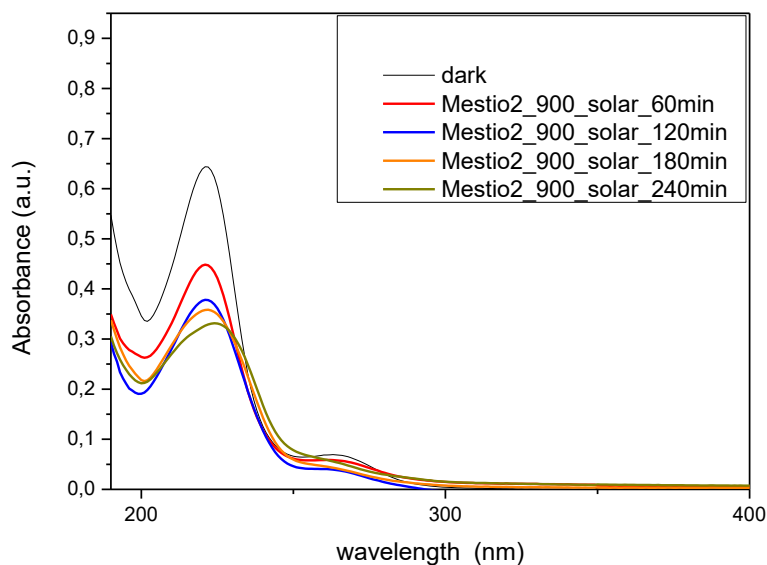


Figure 5.8 MesTiO₂_900 in simazine solution under solar simulated lamp

We reported spectra regarding samples analysed with 60 minutes difference between them to underline reaction going on inside reactor because in this case is possible to follow a consequential pathway between spectra (time-dependent simazine degradation). Dark yellow curve shows a sharp decrease of 221 nm peak and it is possible to observe a band broadening, probably ascribable to the convolution of more than one band. More than one by-products were generated.

5.3.6 Solution n°2 B1_200

In this experiment, we used 50 mL of simazine solution ($1.73\text{E-}5\text{ M}$) in presence of 1g/L of B1_200. Aliquots of the sample were withdrawn every 60 min and all of them are reported in the spectra except for 120min.

Fig 5.9 shows UV-Vis spectra of photocatalytic test with B1_200 powder dispersed in solution n°2 with solar simulated lamp light.

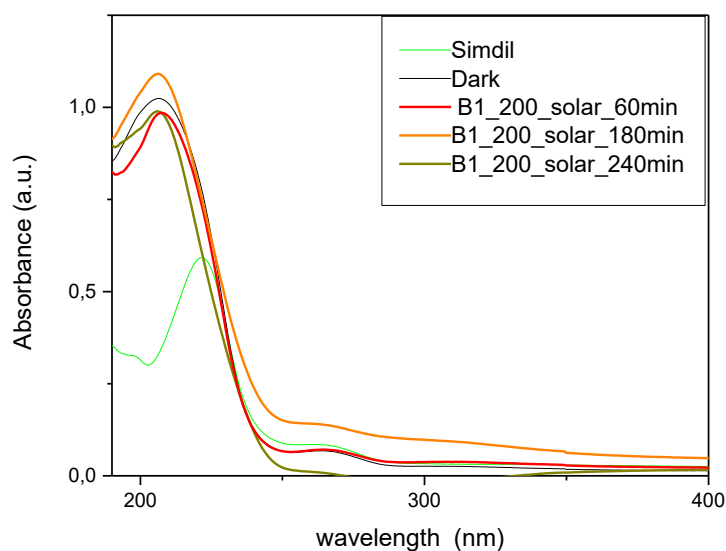


Figure 5.9 B1_200 simazine solution under simulated solar lamp

Photocatalytic efficiency is difficult to understand because all the curves show a similar behaviour. Some shape changes in spectra occur in areas around 250 nm and 200 nm. At high wavelength non-equilibrium reaction, take place as is possible to observe when 180 min and 240 min curves are compared.

5.3.7 Solution n°2 B1_200 Subtracted

In this experiment, we used 50 mL of simazine solution (1.73×10^{-5} M) in presence of 1g/L of B1_200. Aliquots of the sample were withdrawn every 60 min. We reported only 60 min and 180 min

Test condition are the same of paragraph 5.3.5 but here we reported the spectra in Fig 5.10 are resulted after the subtraction with the equivalent blank measurement where 1g/L of B1_200 is dispersed in bi-distilled water and simulated solar lamp is utilised. Aliquots of the solution were withdrawn every 60 min like in common procedure case

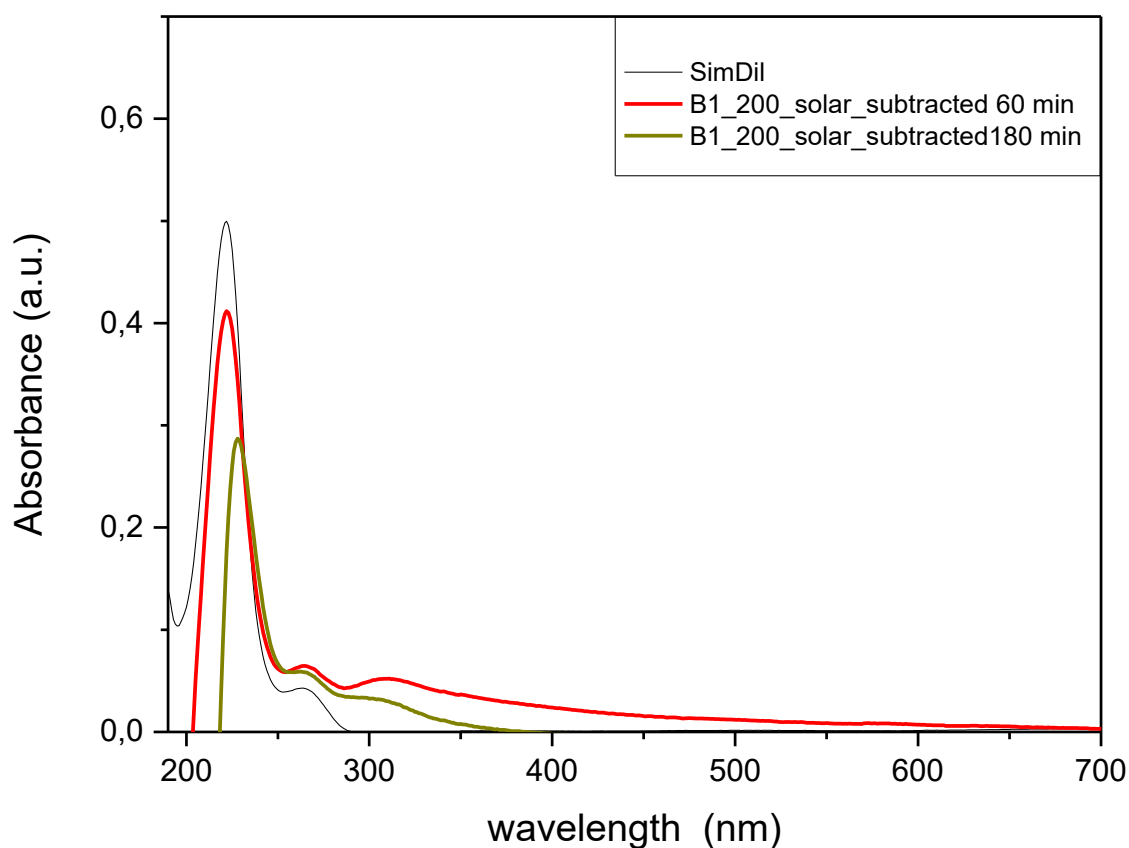


Figure 5.10 Solution n°2 B1_200 Subtracted solar simulated lamp

Fig 5.10 shows a high photocatalytic efficiency similar to the Degussa P25 (paragraph 5.3.3). Dark yellow curve shows a sharp decrease of 221nm peak with an evident red shift that may suggest dechlorination- hydroxylation reaction is taking place.

5.3.8 Solution n°2 B1_200_600

In this experiment, we used 50 mL of simazine solution ($1.73\text{E-}5\text{ M}$) in presence of 1g/L of B1_200_600. Aliquots of the sample were withdrawn every 60 min. We reported only 60 min and 180 min

.Fig 5.11 shows UV-Vis spectra of B1_200_600 photocatalytic test.

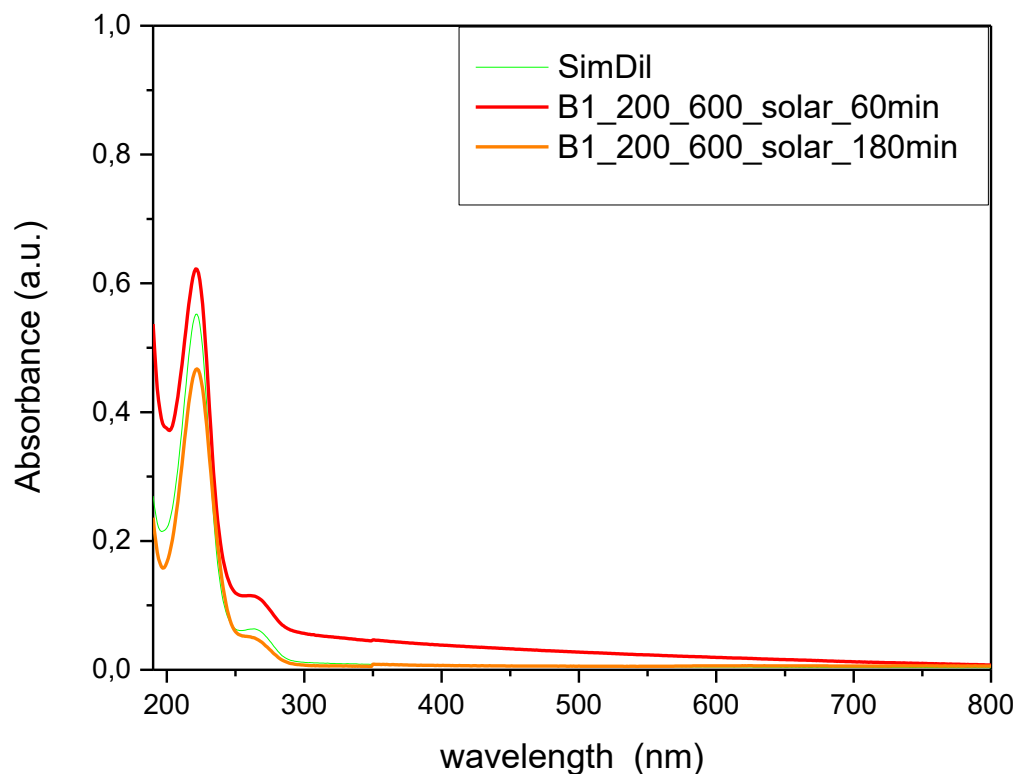


Figure 5.11 B1_200_600 simazine solution solar simulated lamp

Fig 5.11 shows that in presence of B1_200_600 photo-catalyst, the main band of the simazine shows only a decrease in the intensity without any peak position shift. After three hours of illumination, there is a decrease of absorbance (28%) with wavelength corresponding to 200 nm .

5.3.9 Solution n°2 B1_600

In this experiment, we used 50 mL of simazine solution (1.73×10^{-5} M) in presence of 1g/L of B1_600. Aliquots of the sample were withdrawn every 60 min. We reported only 60 min and 240 min

Fig 5.12 shows UV-Vis spectra of B1_600 photocatalytic test.

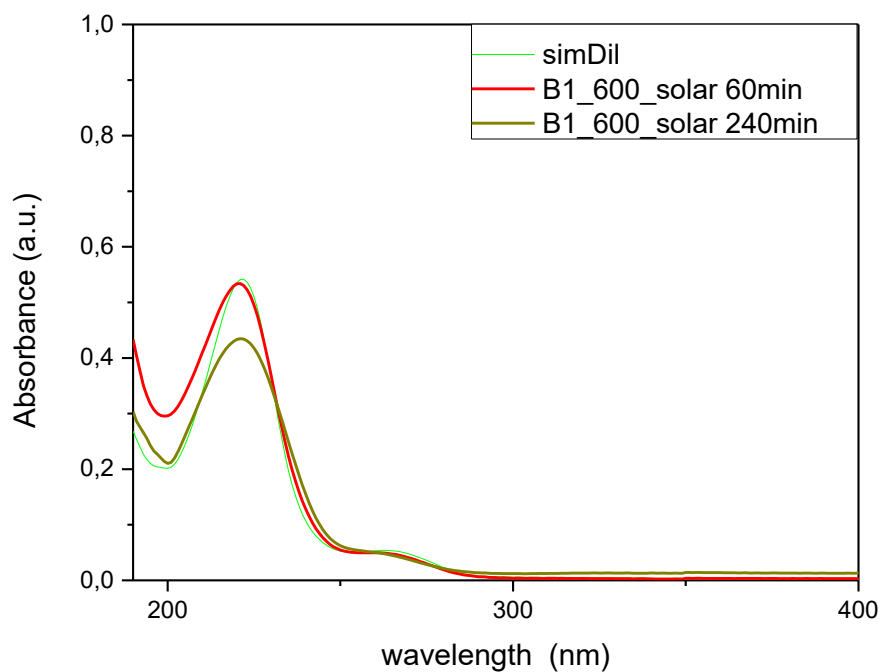


Figure 5.12 B1_600 simazine solution solar simulated lamp

B1_600 test (fig 5.12) shows that the main band of the simazine exhibit only a decrease in the intensity without any peak position shift. After 4 hours of illumination is possible to observe peak shape broadening probably ascribable to the convolution of more than one band.

5.3.10 Solution n°2 B1_200 0,5g/L

In this experiment, we used 50 mL of simazine solution ($1.73\text{E-}5\text{ M}$) in presence of 0,5g/L of B1_200. Aliquots of the sample were withdrawn every 60 min.

Spectra proposed in Fig 5.13 are the resultant spectra after the subtraction with the equivalent blank measurement where 0,5g/L of B1_200 is dispersed in bi-distilled water. Results are proposed below

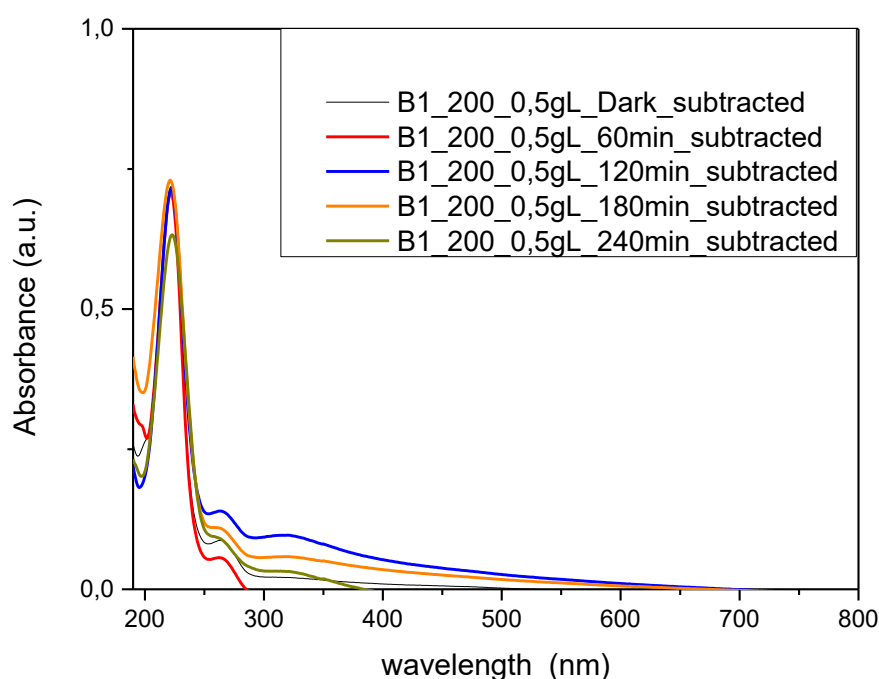


Figure 5.13 B1_200, 0,5g/L in simazine solution under solar simulated lamp

Fig 5.12 shows change in absorbance of both side of 221nm spectra. Shape change among curves in correspondence of 300 nm may be due to nitrates formation. The main band of the simazine at 221 nm shows only a decrease in the intensity without any peak position shift. Main band absorbance decreased of 11% after 240 min irradiation

5.4 Solution n°2 MesTiO₂_450 UV

In this experiment, we used 50 mL of simazine solution (1.73E-5 M) in presence of 0,5g/L of MesTiO₂_450. Aliquots of the sample were withdrawn every 60 min.

UV lamp has been proposed to test our sample in different analysis condition. Fig 5.14 shows UV-Vis spectra of UV- MesTiO₂_450 test

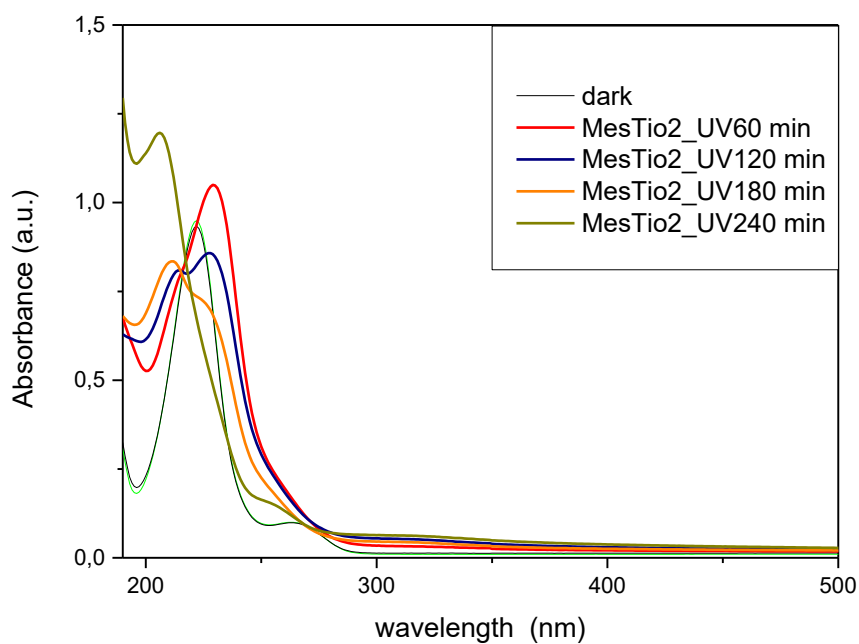


Figure 5.14 MesTiO₂_450 in simazine solution under UV lamp

Fig 5.14 the main band of the simazine at 221 nm shows shape and steep change. Main simazine band shows position shift as well. All these variations of curves and peaks are due to simazine degradation.

Conclusions

Our work focused on numerous aspects of photo catalysis processes, such as the crystalline phase of the photo catalyst, kind of light source and doping. As photo catalyst, we chose titanium dioxide, one of the most applied photo catalyst.

TiO₂ properties were investigated and tuned to optimize it for degradation of nitrogen containing pollutants in aqueous solution.

Nitrogen containing pollutants selected for photocatalytic tests were herbicides from the triazine family, which is a class of nitrogen-containing heterocycles, where a planar benzene-like aromatic ring has three nitrogen's atoms replacing carbons atoms. Among triazine we selected simazine molecule C₇H₁₂ClN₅ .

Photocatalytic materials were synthesised by two main synthesis methods. The two methods mainly differ from each other for the use of a soft template during the synthesis process: while the first proposed method uses a triblock copolymer, the second proposed method does not apply any template but the particle formation is based on pH changes.

Different temperatures of calcination were applied to tune material properties and obtain different crystallographic polymorphisms.

We tested photocatalytic properties of many configuration:

- Anatase structure (MesTiO₂_450 and MesTiO₂_700).
- Anatase-rutile structure (MesTiO₂_900)
- Anatase-rutile-brookite (B1_200, B1_200_600, B1_600)
- Anatase structure doped with Fe (MesTiO₂dirFe)

Among parameters that influence the photocatalytic properties of a material, we focused on three main aspects:

- Band gap of materials
- Morphological properties of materials
- Crystallographic structure of materials

These three properties can influence each other during the photocatalytic process.

Energy band gap can be modified by adding doping atoms and by changing crystalline properties of the semiconductor as demonstrated in chapter 4, where energy band gap are listed.

We demonstrate that materials with similar crystallographic composition and comparable morphological properties have similar band gap energy obtained with DR-UV-Vis analysis (i.e. B1_600 and B1_200_600).

Another important aspect, in photo catalysis studies, is electron-hole recombination rate. During our work, numerous crystallographic structures were proposed to delay this phenomenon. According to literature, since multi-crystallographic phases should delay recombination between carriers, we proposed and tested mostly materials that show three or

two crystallographic phases. XRPD technique was utilized to analyse sample crystallographic composition.

Materials superficial properties were investigated with BJH porosity distribution and BET surface area. Crystallites dimension were examined with TEM images elaboration.

Materials produced with classical sol gel method showed mesoporous structure. When material undergoes calcination at 900°C Crystallographic phase transition (anatase to rutile) and morphological changes occurs. Synthesis method without template usage led to mesoporous materials

Photocatalytic tests have been carried out by using commercial Degussa P25 (P25) catalyst as a term of comparison. P25 crystallographic structure is composed by a mixture of rutile and anatase phases (81%-19%). P25 presents low porosity structure and BET specific surface area of 50 m²/g.

Experimental setting for photocatalytic test was described in chapter 3.

During our tests with solar simulated lamp irradiation, P25 induced dechlorination-hydroxylation of simazine in presence of hydrogen peroxide. Comparable results were obtained B1_200 sample was utilised as photo catalyst under the same photocatalytic condition. In latter case, no H₂O₂ was utilized. This result is very promising because P25 is worldwide known for its efficiency and our material showed comparable results.

B1_200 high efficiency can be attributed to high surface area compared to P25 (no-porous material).

In order to confirm B1_200 efficiency we carried out photocatalytic tests with 0,5g/L catalyst concentration instead of 1g/L. Good efficiency in pollutant degradation was demonstrated even in these cases.

During our investigation work we found some problems during B1_200 analysis. FTIR spectroscopy investigation showed presence of organic compound on powder surface. Organic pollutant are a consequence of synthesis precursor and low calcination temperature.

Other catalyst that showed efficient photocatalytic properties is MesTiO₂_900 despite of its low specific surface area and porosity. Simazine considerable degradation has been achieved without hydrogen peroxide.

Photocatalytic test with Fe doped catalyst (MesTiO₂dirFe) showed considerable degradation of simazine thanks to band gap reduction and synergic effect when utilized with hydrogen peroxide.

Photocatalytic tests results showed strong influence of crystallographic phases and morphological properties of materials on their photocatalytic properties.

In summary, we proposed some TiO₂-based photo catalyst and synthesis methods to degrade nitrogen based pollutants but no total mineralization was achieved with our materials and analysis settings.

Future perspective could be a better understanding of photocatalytic process intermediaries and by-products. In order to detect these molecules other analytical techniques, like HPLC (high performance liquid chromatography) could be applied. With this purpose we have started a

collaboration with professor Tanveer Ahmed at U.S.-Pakistan Centers for Advanced Studies in Water.

These materials could be also tested for the photo catalysis of other emerging pollutants. For this, we have started a collaboration to professor Vincenzo Vaiano of Università di Salerno. Professor Vaiano will test our samples in presence of caffeine, another emerging contaminant.

Bibliography

- [1] F. Freyria, F. Geobaldo, and B. Bonelli, "Nanomaterials for the Abatement of Pharmaceuticals and Personal Care Products from Wastewater," *Appl. Sci.*, vol. 8, no. 2, p. 170, 2018.
- [2] "Catalyst," *IUPAC Compend. Chem. Terminol.*, vol. 2291, no. Recommendations 1990, p. 2293, 2014.
- [3] F. S. Freyria, M. Armandi, M. Compagnoni, G. Ramis, I. Rossetti, and B. Bonelli, "Catalytic and Photocatalytic Processes for the Abatement of N-Containing Pollutants from Wastewater. Part 2: Organic Pollutants," *J. Nanosci. Nanotechnol.*, vol. 17, no. 6, pp. 3654–3672, 2017.
- [4] H. K. Fujishima A, "© 1972 Nature Publishing Group," *Nature*, vol. 238, 1972.
- [5] P. Pichat, *Functional Nanostructured Materials and Membranes for Water Treatment Risk Analysis of Water Pollution Photocatalysis Activated Carbon for Water and Wastewater Treatment Biological Wastewater Treatment Ozonation of Water and Waste Water*. 2013.
- [6] D. Friedmann, C. Mendive, and D. Bahnemann, "TiO₂ for water treatment: Parameters affecting the kinetics and mechanisms of photocatalysis," *Appl. Catal. B Environ.*, vol. 99, no. 3–4, pp. 398–406, 2010.
- [7] I. Medina-Ramirez and A. Hernandez-Ramirez, *Photocatalytic Semiconductors*. Springer, 2015.
- [8] A. Di, E. García-lópez, G. Marci, and L. Palmisano, "A survey of photocatalytic materials for environmental remediation," *J. Hazard. Mater.*, vol. 221–212, pp. 3–29, 2012.
- [9] A. A. K. Momeni, A. P. Y. K. Yap, and R. S. Yassar, "On the correlation of crystal defects and band gap properties of ZnO nanobelts," pp. 909–914, 2011.
- [10] M. Hara, T. Kondo, M. Komoda, S. Ikeda, K. Shinohara, and A. Tanaka, "Cu₂O as a photocatalyst for overall water splitting under visible light irradiation," vol. 2, pp. 357–358, 1998.
- [11] A. Paracchino, V. Laporte, K. Sivula, M. Grätzel, and E. Thimsen, "Highly active oxide photocathode for photoelectrochemical water reduction," *Nat. Mater.*, vol. 10, no. 6, pp. 456–461, 2011.
- [12] M. A. Gondal, "Activity comparison of Fe₂O₃, NiO, WO₃, TiO₂ semiconductor catalysts in phenol degradation by laser enhanced photo-catalytic process," vol. 445, pp. 325–330, 2007.
- [13] J. Ren, W. Wang, L. Zhang, J. Chang, and S. Hu, "Photocatalytic inactivation of bacteria by photocatalyst Bi₂WO₆ under visible light," *Catal. Commun.*, vol. 10, no. 14, pp. 1940–1943, 2009.
- [14] R. Asahi, T. Morikawa, H. Irie, and T. Ohwaki, "Nitrogen-doped titanium dioxide as visible-light-sensitive photocatalyst: Designs, developments, and prospects," *Chem. Rev.*, vol. 114, no. 19, pp. 9824–9852, 2014.
- [15] C. Y. Wang, C. B. Ttcher, D. W. Bahnemann, and J. K. Dohrmann, "A comparative study of nanometer sized Fe(III)-doped TiO₂ photocatalysts: Synthesis, characterization

- and activity,” *J. Mater. Chem.*, vol. 13, no. 9, pp. 2322–2329, 2003.
- [16] W. Jiao *et al.*, “Synthesis of mesoporous single crystal rutile TiO₂ with improved photocatalytic and photoelectrochemical activities,” *Chem. Commun.*, vol. 49, no. 100, p. 11770, 2013.
- [17] S. Shen *et al.*, “Titanium dioxide nanostructures for photoelectrochemical applications,” *Prog. Mater. Sci.*, vol. 98, no. May, pp. 299–385, 2018.
- [18] J. Zhang, P. Zhou, J. Liu, and J. Yu, “New understanding of the difference of photocatalytic activity among anatase, rutile and brookite TiO₂,” *Phys. Chem. Chem. Phys.*, vol. 16, no. 38, pp. 20382–20386, 2014.
- [19] T. A. Kandiel, L. Robben, A. Alkaim, and D. Bahnemann, “Brookite versus anatase TiO₂ photocatalysts: Phase transformations and photocatalytic activities,” *Photochem. Photobiol. Sci.*, vol. 12, no. 4, pp. 602–609, 2013.
- [20] B. Ohtani, J. ichi Handa, S. ichi Nishimoto, and T. Kagiya, “Highly active semiconductor photocatalyst: Extra-fine crystallite of brookite TiO₂ for redox reaction in aqueous propan-2-ol and / or silver sulfate solution,” *Chem. Phys. Lett.*, vol. 120, no. 3, pp. 292–294, 1985.
- [21] J. J. M. Vequizo, H. Matsunaga, T. Ishiku, S. Kamimura, T. Ohno, and A. Yamakata, “Trapping-Induced Enhancement of Photocatalytic Activity on Brookite TiO₂ Powders: Comparison with Anatase and Rutile TiO₂ Powders,” *ACS Catal.*, vol. 7, no. 4, pp. 2644–2651, 2017.
- [22] M. Cargnello, T. R. Gordon, and C. B. Murray, “Solution-phase synthesis of titanium dioxide nanoparticles and nanocrystals,” *Chem. Rev.*, vol. 114, no. 19, pp. 9319–9345, 2014.
- [23] K. Byrappa and M. Yoshimura, *Handbook of Hydrothermal Technology*. 2013.
- [24] A. A. Ismail and D. W. Bahnemann, “Mesoporous titania photocatalysts: Preparation, characterization and reaction mechanisms,” *J. Mater. Chem.*, vol. 21, no. 32, pp. 11686–11707, 2011.
- [25] M. Grassi, G. Kaykioglu, and V. Belgiorno, “Emerging Compounds Removal from Wastewater,” pp. 15–38, 2012.
- [26] R. Andreozzi, V. Caprio, A. Insola, and R. Marotta, “Advanced oxidation processes (AOP) for water purification and recovery,” vol. 53, pp. 51–59, 1999.
- [27] E. Pellizzetti *et al.*, “Photocatalytic Degradation of Atrazine and Other s-Triazine Herbicides,” *Environ. Sci. Technol.*, vol. 24, no. 10, pp. 1559–1565, 1990.
- [28] U. I. Gaya and A. H. Abdullah, “Heterogeneous photocatalytic degradation of organic contaminants over titanium dioxide: A review of fundamentals, progress and problems,” *J. Photochem. Photobiol. C Photochem. Rev.*, vol. 9, no. 1, pp. 1–12, 2008.
- [29] I. Oller, S. Malato, and J. A. Sánchez-Pérez, “Combination of Advanced Oxidation Processes and biological treatments for wastewater decontamination-A review,” *Sci. Total Environ.*, vol. 409, no. 20, pp. 4141–4166, 2011.
- [30] T. A. McMurray, P. S. M. Dunlop, and J. A. Byrne, “The photocatalytic degradation of atrazine on nanoparticulate TiO₂ films,” *J. Photochem. Photobiol. A Chem.*, vol. 182, no. 1, pp. 43–51, 2006.

- [31] F. J. Rivas, V. Navarrete, F. J. Beltrán, and J. F. García-Araya, "Simazine Fenton's oxidation in a continuous reactor," *Appl. Catal. B Environ.*, vol. 48, no. 4, pp. 249–258, 2004.
- [32] S. E. Hatfield, "Applications of Triazine Chemistry : Education , Remediation , and Drug Delivery Applications of Triazine Chemistry : Education , Remediation , and Drug Delivery," no. May, 2007.
- [33] C. Chen, S. Yang, Y. Guo, C. Sun, C. Gu, and B. Xu, "Photolytic destruction of endocrine disruptor atrazine in aqueous solution under UV irradiation: Products and pathways," *J. Hazard. Mater.*, vol. 172, no. 2–3, pp. 675–684, 2009.
- [34] C. L. Elmore and A. H. Lange, *Triazine Herbicides for Weed Control in Fruit and Nut Crops*. Elsevier B.V., 2008.
- [35] E. Evgenidou and K. Fytianos, "Photodegradation of triazine herbicides in aqueous solutions and natural waters," *J. Agric. Food Chem.*, vol. 50, no. 22, pp. 6423–6427, 2002.
- [36] R. G. Zepp and D. M. Cline, "Rates of Direct Photolysis in Aquatic Environment," *Environ. Sci. Technol.*, vol. 11, no. 4, pp. 359–366, 1977.
- [37] A. C. Bethsass, "European Union Bans Atrazine, While the United States Negotiates Continued Use," *J. Occup. Environ. Heal.*, vol. 12, no. 3, pp. 260–267.
- [38] M. Thommes *et al.*, "Physisorption of gases, with special reference to the evaluation of surface area and pore size distribution (IUPAC Technical Report)," *Pure Appl. Chem.*, vol. 87, no. 9–10, pp. 1051–1069, 2015.
- [39] J. M. H. A. Sclafani, "Comparison of the Photoelectronic and Photocatalytic Activities of Various Anatase and Rutile Forms of Titania in Pure Liquid Organic Phases and in Aqueous Solutions," *J. Phys. Chem.*, 1996, 100 (32), pp, vol. 100, no. 32, pp. 13655–13666, 1996.
- [40] S. Brunauer, P. H. Emmett, and E. Teller, "Adsorption of Gases in Multimolecular Layers," *J. Am. Chem. Soc.*, vol. 60, no. 2, pp. 309–319, 1938.
- [41] Agilent Te, "UV-visible spectroscopy," *R. Soc. Chem.*, vol. Agilent Te, p. 22, 2000.
- [42] H. Ma, K.-J. Shieh, and T. X. Qiao, "Study of Transmission Electron Microscopy (TEM) and Scanning Electron Microscopy (SEM)," *Nat. Sci.*, vol. 4, no. 3, pp. 14–22, 2006.
- [43] D. B. Williams and C. B. Carter, *Transmission Electron Microscopy, A Textbook for Materials Science*. 2009.
- [44] E. M. Facility and T. November, "FEI Tecnai TM G 2 Spirit Transmission Electron Microscope," no. November, p. 2, 2013.
- [45] N. Colthup, L. Daly, and S. Wiberley, "Vibrational and rotational spectra 1.1," in *Introduction to Infrared and Raman Spectroscopy 3rd Edition*, Third., 1990, p. 547.
- [46] Perkins, "Fourier Transform-Infrared Spectroscopy," vol. 63, no. 1, pp. 5–10, 1986.
- [47] B. K. Mutuma, G. N. Shao, W. D. Kim, and H. T. Kim, "Sol-gel synthesis of mesoporous anatase-brookite and anatase-brookite-rutile TiO₂nanoparticles and their photocatalytic properties," *J. Colloid Interface Sci.*, vol. 442, pp. 1–7, 2015.

- [48] C. Olivan, "Synthesis and characterization of mesoporous titania (either pure or loaded with Fe or V) for catalytic degradation of azo-dyes," Politecnico di Torino, 2015.
- [49] K. Thamaphat, P. Limsuwan, and B. Ngotawornchai, "Tio₂ Xrd Pattern," vol. 361, pp. 357–361, 2008.
- [50] K. J. A. Raj and B. Viswanathan, "Surface area p25," vol. 48, no. October, pp. 1378–1382, 2009.
- [51] T. Allen, "Particle Size Measurement," *Nature*, vol. 208, no. 5010, pp. 529–529, 1965.
- [52] W. J. and E. R. L. Hayes, *Handbook of Pesticide Toxicology*, Academic p. NY, 1990.